This document is downloaded from DR-NTU (https://dr.ntu.edu.sg)
Nanyang Technological University, Singapore.

Known and unknown facts of LoRa : experiences from a large-scale measurement study

Liando, Jansen Christian; Gamage, Amalinda; Tengourtius, Agustinus Wellson; Li, Mo

2019

Liando, J. C., Gamage, A., Tengourtius, A. W., & Li, M. (2019). Known and unknown facts of LoRa : experiences from a large-scale measurement study. ACM Transactions on Sensor Networks, 15(2), 16-. doi:10.1145/3293534

https://hdl.handle.net/10356/142869

https://doi.org/10.1145/3293534

© 2019 The Author(s). All rights reserved. This paper was published by ACM in ACM Transactions on Sensor Networks and is made available with permission of The Author(s).

Downloaded on 28 Mar 2024 23:14:06 SGT

Known and Unknown Facts of LoRa: Experiences from a Large-scale Measurement Study

JANSEN C. LIANDO, AMALINDA GAMAGE, AGUSTINUS W. TENGOURTIUS, and MO LI, School of Computer Science and Engineering, Nanyang Technological University, Singapore

Long Range (LoRa) is a Low-power Wide-area Network technology designed for the Internet of Things. In recent years, it has gained significant momentum among industrial and research communities. Patented by Semtech, LoRa makes use of chirp spread spectrum modulation to deliver data with promises of long battery life, far-reaching communication distances, and a high node density at the cost of data rate. In this article, we conduct a series of experiments to verify the claims made by Semtech on LoRa technology. Our results show that LoRa is capable of communicating over 10km under line-of-sight environments. However, under non-line-of-sight environments, LoRa's performance is severely affected by obstructions such as buildings and vegetations. Moreover, the promise of prolonged battery life requires extreme tuning of parameters. Last, a LoRa gateway supports up to 6,000 nodes with PRR requirement of >70%. This study also explores the relationship between LoRa transmission parameters and proposes an algorithm to determine optimal settings in terms of coverage and power consumption under non-line-of-sight environments. It further investigates the impact of LoRa Wide-area Networks on energy consumption and network capacity along with implementation of a LoRa medium access mechanism and possible gains brought forth by implementing such a mechanism.

CCS Concepts: • **Networks** → **Network performance analysis**; **Network measurement**; **Wide area networks**; Sensor networks;

Additional Key Words and Phrases: Network measurement, network performance analysis, sensor networks, wide-area networks, low-power wide-area network, internet of things, LoRa

ACM Reference format:
Jansen C. Liando, Amalinda Gamage, Agustinus W. Tengourtius, and Mo Li. 2019. Known and Unknown Facts of LoRa: Experiences from a Large-scale Measurement Study. *ACM Trans. Sen. Netw.* 15, 2, Article 16 (February 2019), 35 pages.
https://doi.org/10.1145/3293534

1 INTRODUCTION

Low-power Wide-area Networks (LPWANs) are garnering increased attention from the research community and is expected to be the missing piece for the future scalable Internet of Things (IoT).

This work is supported by Singapore MOE Tier 2 Grant No. MOE2016-T2-2-023, Tier 1 Grant No. 2017-T1-002-047, and NTU CoE Grant No. M4081879.
Authors' address: J. C. Liando, A. Gamage, A. W. Tengourtius, and M. Li, School of Computer Science and Engineering, Nanyang Technological University, 50 Nanyang Avenue, Singapore, 639798, Singapore; emails: {cjansen, amalinda, atengourtius, limo}@ntu.edu.sg.
Permission to make digital or hard copies of all or part of this work for personal or classroom use is granted without fee provided that copies are not made or distributed for profit or commercial advantage and that copies bear this notice and the full citation on the first page. Copyrights for components of this work owned by others than the author(s) must be honored. Abstracting with credit is permitted. To copy otherwise, or republish, to post on servers or to redistribute to lists, requires prior specific permission and/or a fee. Request permissions from permissions@acm.org.

Recent new LPWAN developments are aimed at fulfilling the gaps composed of limitations to battery life, coexistence, and communication range of IoT devices.

Long Range (LoRa) is a recent industry initiated LPWAN technology by Semtech among these efforts in building a scalable IoT. LoRa, shortly after its release, captured considerable attention from scientific and industrial communities and brought together multilateral efforts with strong potential to collaborate on the development of worldwide coverage for IoT devices.

LoRa's popularity stems from a range of features and performance promises. First, LoRa utilizes the unlicensed Industrial, Scientific, and Medical radio (ISM) bands and promises kilometers of communication distance and several years of battery life. Second, LoRa incorporates a variation of Chirp Spread Spectrum (CSS) [17] technology that Semtech claims to be robust against a high degree of interference in addition to multi-path and Doppler effects [2, 34, 41]. Third, LoRa also claims to support high channel capacity, meaning that a single channel supports simultaneous transmissions from multiple devices, which is in high contrast to conventional LPWAN technologies. Although LoRa's physical layer is a proprietary technology acquired by Semtech [51, 52], parts from the same are open to the public [11, 34]. In this article, we exploit the public information to widen the existing knowledge on LoRa. Despite clinging to claims printed on data sheets, our measurement study tests such claims with practical conditions and real-life scenarios. We perform experimental investigations to further understand the capacity to optimize and improve LoRa's performance in various ways. Our study aims at answering researchers or system adopters' questions, such as: "What are the most energy-efficient LoRa configurations under different distance and environment conditions?"; "How can the upper LoRaWAN MAC behaviors have an impact on the LoRa system performance in terms of the energy and channel efficiency?"; "What is the LoRa PHY efficiency?"; "How can we improve in terms of medium access efficiency, reliability, robustness, and so on?"

We primarily experiment with our campus deployment composed of handcrafted LoRa gateways deployed on the rooftops of three buildings, a LoRa network server at the cloud side, 50+ end nodes tested with various conditions, a mobile LoRa gateway, as well as various wireless spectrum sensing and data logging devices. The measurement study is performed within an area of 3×3km, comprising the university campus and nearby residential region. This study collected and analyzed >100 sensor traces with >2,000,000 lines of data. To reveal the PHY details of LoRa, we further build a software defined radio (SDR) enabled LoRa gateway based on USRP N210 and GNU Radio, with which we can intercept on-the-air LoRa transmissions and perform PHY-level signal analysis.

This article is organized as follows. Section 2 briefly introduces fundamentals of LoRa modulation and our experimental setup. Section 3 reports our measurement findings and derived models in accordance with the performance promises by LoRa. Section 4 exploits the optimization and improvement opportunities and explores beyond existing scope of LoRa practices by gaining insights through SDR-based LoRa PHY analysis. Section 5 discusses some other LoRa measurement studies and concludes this article.

2 OVERVIEW OF LORA

We briefly introduce LoRa modulation and the key technical parameters to establish a common understanding to better comprehend Sections 3 and 4. In LoRa, chirp and symbol both refer to the modulated signal that carries data, and in this article, we use them interchangeably.

2.1 LoRa Modulation

LoRa employs CSS modulation to modulate signals. A chirp in CSS refers to a signal with constantly increasing or decreasing frequency that sweeps through and wraps around a predefined bandwidth, referred to as *upchirps* and *downchirps*. Figure 1 visualizes a LoRa packet captured

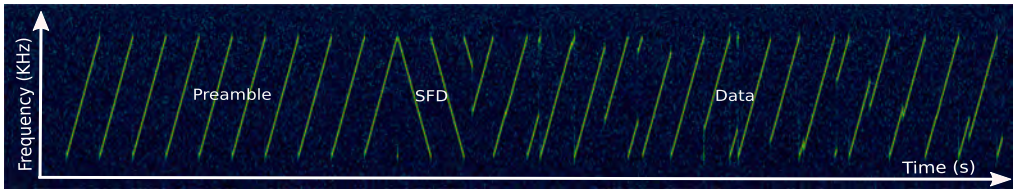


Fig. 1. A snapshot of LoRa transmission that shows up, down, and data chirps as seen on spectrogram.

using a software defined radio setup from our experiment. The figure illustrates different types of chirps—the first half being standard *upchirps* where frequency increases over time and restarts from the min frequency (f_{min}) toward max frequency (f_{max}), followed by short *downchirps* annotated as Start Frame Delimiter (SFD) that goes from f_{max} to f_{min}, and then modulated chirps that contain data bits.

The simplest implementation of CSS is *on-off keying*, which modulates data into *upchirps* and *downchirps*. The LoRa implementation of CSS, however, differs from that and modulates data through the changes in the chirp's starting frequency position. The instantaneous change in the starting frequency indicates the symbol border as illustrated in the modulated chirps in Figure 1.

Theoretically, LoRa is able to achieve a data rate up to 27kbit/s. The data rate, while limited, is more than sufficient for LPWAN applications where communication coverage is prioritized over data rate. LoRa configuration can be modified by manipulating some key parameters to achieve trade-offs among communication distances, data rate, and power consumptions.

2.2 Key Parameters

LoRa employs a unique variation of Chirp Spread Spectrum modulation, which incorporates four key parameters: channel, bandwidth, spreading factor, and transmission power. As depicted in Figure 1, LoRa utilizes a combination of *upchirps* and *downchirps* to formulate a full packet. The angle of chirps, known as the spreading factor, remains consistent throughout the packet. For a system with constant frequency bandwidth, the spreading factor determines the final data rate. LoRa modulation, at the time, supports seven different spreading factors ranging from SF6 to SF12. SF6 having the highest data rate requires the highest signal-to-noise ratio (SNR) for successful demodulation while SF12 supports lowest data rate but requires lowest SNR for the same transmission power.

A chirp's gradient is determined by predefined parameters offered by Semtech's LoRa transceiver, which includes the spreading factor (SF) and frequency bandwidth (BW). The relationship of SF and BW is explained in Reference [34] where each chirp consists of 2^{SF} number of RF chips carrying SF number of data bits. The number of chips that formulate a complete chirp is directly proportional to BW and is computed as a chip per Hz of BW. Therefore, a standard LoRa chirp that sweeps a BW of 125KHz comprises of 125,000 chips/s. The duration T_{sym} of such a chirp is given in Equation (1):

$$T_{sym} = \frac{2^{SF}}{BW}. \tag{1}$$

In addition to controlling data rate, the diversity of spreading factor choices also increases coexistence of LoRa devices, i.e., uniquely different chirp gradients (different SFs) allow the demodulator to develop a factor of resilience against simultaneous transmissions of different SFs in the same channel and demodulate all of them. Such a feature significantly enhances the multiple access efficiency of LoRa, which we comprehensively tested and report in Sections 3 and 4.

Semtech LoRa chipset [58] sets a fixed number of options for each parameter as listed in Table 1 along with the recommended guidelines for using each parameter. The most prominent

Table 1. Configuration Options Provided by Semtech LoRa Chipset

Parameter	Options
SF	6, 7, 8, 9, 10, 11, 12
BW (kHz)	7.8, 10.4, 15.6, 20.8, 31.2, 41.7, 62.5, 125, 250, 500
CR	4/5, 4/6, 4/7, 4/8
IH	True or False
DE	True or False (recommended True for $T_{sym} > 16$ms)
CRC	True (*uplink*) or False (*downlink*)
PL	0–255 Bytes
S_{pre}	6–65,535 symbols

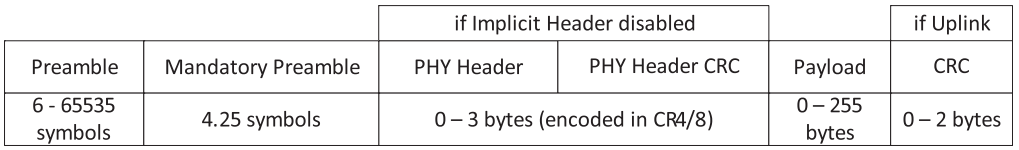


Fig. 2. LoRa PHY packet structure.

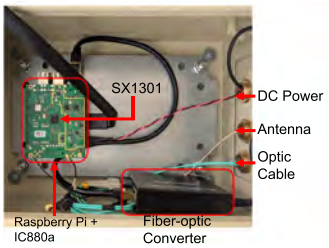
recommendation made by Semtech is to use SF settings of SF7 to SF12 and BW 125, 250, and 500kHz [31]. Those recommendations were given to ensure the acceptable transmission distance and data rate trade-off as both SF and BW would affect transmission duration and data rate.

The LoRa packet structure is separated into *uplink* and *downlink* packets, which is indicated by the presence and absence of packet cyclic redundancy check (CRC). The number of symbols to be transmitted in a packet is heavily dependent on SF except for the set number of preamble symbols (S_{pre}) and start frame delimiter (SFD) symbols. A LoRa packet consists of S_{pre} preamble symbols, 2 mandatory sync word symbols, 2.25 SFD symbols, and based on SF, a variable number of data chirps.

For LoRa physical header and payload, LoRa chirps imposes another set of parameters including code rate (CR), implicit header (IH), low data rate optimization enabled (DE), and existence of CRC on top of SF. CR determines error correction capability, which is based on Hamming code. The CR setting is represented as $4/x$, which indicates 4 information bits padded with $x - 4$ number of parity bits. As illustrated in Figure 2, The PHY header can be excluded by enabling IH (setting IH to 1). However, the DE parameter adds another layer of redundancy to the data bits for any LoRa transmission when T_{sym} exceeds 16ms. The existence of CRC at the end of the packet can be controlled through the CRC flag and is usually modified to differentiate between *uplink* and *downlink* packets. LoRa packet size is limited to 255 Bytes, which can be indicated by the single Byte payload size (b_{pl}) field in the PHY header.

2.3 Experiment Setup

The system setup incorporates three LoRa gateways located within the area of 1×1km on top of three buildings on campus (the deployments indicated in Figure 4). Each gateway is handcrafted and built with a Raspberry-Pi and an IMST IC880A [23], which works as a radio frontend similar to the design in Reference [7]. The antenna connected to the gateway has 4dBi gain and the Raspberry-Pi executes a single thread of either the *LoRa Packet Forwarder* or *LoRa Packet Logger* as required by different experiment purposes [10, 16]. A picture of the gateway hardware is shown in Figure 3(a).



(a) The handcrafted LoRa gateway developed with IC880A frontend and Raspberry-Pi enabled processing unit.



(b) The LoRa end node developed with SX1276 frontend (inAir9B [24]) and ATMEGA328P processing unit.



(c) The software defined radio based LoRa gateway developed with USRP N210 and RFX900 daughterboard.

Fig. 3. Hardware utilised for the experimental system.

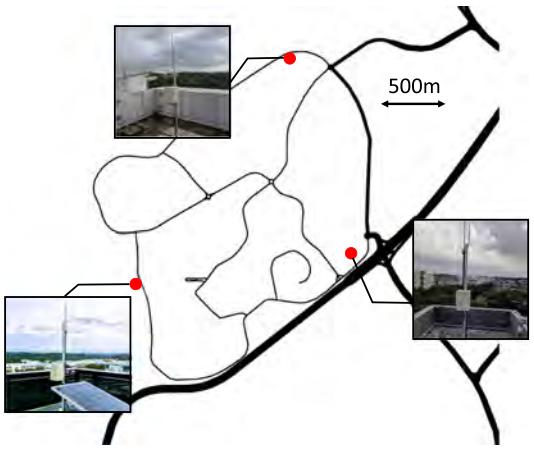


Fig. 4. Gateway locations placed within the campus grounds.

More than 50 LoRa end nodes similar to the design found in [27] are utilized throughout the experiment and tested over an area of over 3 × 3km comprising the university campus and nearby region of residences. Each node is composed of an Arduino Pro Mini (ATMEGA328P) working as the processing unit interfaced with SX1276 working as the radio frontend. Unnecessary components such as voltage regulators and LEDs were taken off the end nodes to ensure high accuracy of power measurements. An image of such an end node is given in Figure 3(b). Power profiling for end nodes is achieved using the Monsoon Power Monitor [46] that measures the power at an accuracy of 10^6 samples/s. We also implement the LoRa gateway functionality with software defined radio (based on USRP N210 [61] and GNU Radio [49]), and utilize the SDR gateway to intercept on-the-air LoRa transmissions and perform PHY-level signal analysis. Figure 3(c) depicts the SDR gateway settings.

3 PROMISES OF LORA

This section reports our experiment results to verify the performances promised by LoRa. We further derived models to describe LoRa's performance by varying existing parameters provided by Semtech chipsets.

3.1 Communication Distance

One of the key factors in enabling scalable IoT system is the communication distance of end devices, and in this case, Semtech has promised an ultra-long range connectivity for LoRa devices [58]. In this section, we quantify the ultra-long range of LoRa devices in various environments.

Parameter Impact

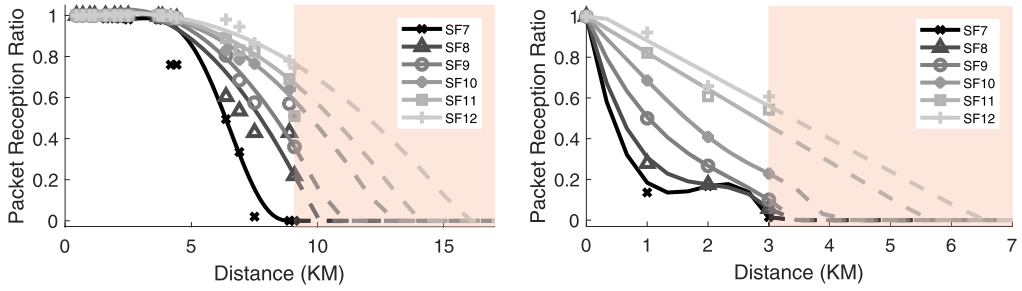
LoRa transmission distance could be affected by the underlying parameter selection. To understand the impact of each parameter, we first need to understand the effect of each parameter in shaping the resulting wireless signals. There are four main parameters with pronounced effect on LoRa signals. These parameters are listed below:

3.1.1 Spreading Factor (SF). Spreading Factor in LoRa refers to a value that determines how spread out the chirp would be. This level of spread-ness is mainly due to the number of bits crammed into a single chirp. For example, SF7 means that each chirp represents seven bits. As LoRa chirp is modulated by varying the starting/ending frequency of each chirp, there has to be 2^{SF} number of starting/ending frequency position. Recall in Section 2, a chirp has to sweep through a given bandwidth and the time duration for a chirp can be determined through Equation (1), where the time taken for a chirp frequency to increase/decrease from f_{SF}^{i} to f_{SF}^{i+1} or f_{SF}^{i-1} is $\frac{1}{BW}$s and this is referred to as a chip in Reference [34]. A chirp is formed by going through all possible f_{SF}, which results in 2^{SF} number of chips. In this case, with every increment of SF, the time taken to transmit a chirp is effectively doubled assuming all the other parameters remains the same. By doubling the chirp duration, receivers would have more opportunities to sample the signal power, which results in higher signal-to-noise ratio (SNR). Since the definition of SNR is $\frac{P_{signal}}{P_{noise}}$, the higher the signal power P_{signal} as compared to noise power P_{noise} is, the higher the probability of each chirp to be received correctly.

3.1.2 Bandwidth (BW). Bandwidth, however, determines the width of the transmitted signal and according to Equation (1), BW would also determine chirp duration. Remember that a chirp consists of 2^{SF} number of chips and the duration of each chip is $\frac{1}{BW}$. By changing the BW, chip duration would change accordingly, which in turn affects the chirp duration and finally the SNR or that particular chirp. LoRa gateway chipset are optimized to receive transmission of 125kHz with added option in receiving transmission of a fixed SF with varying BW (250 and 500kHz) and GFSK (Gaussian Frequency Shift Keying) transmissions.

3.1.3 Transmission Power (TX Pow). Transmission power directly affects the amount of power used to transmit a chirp. By increasing TX Pow, the signal will have higher chances of surviving attenuation caused by the environment, which effectively increases the signal power P_{signal} received by receivers. Semtech gateway chipset SX1301 [59] claims a −142dBm sensitivity and is capable of operating even with negative SNR of up to 9dB, which means it is able to operate even if the transmitted signal is below the noise floor.

3.1.4 Code Rate (CR). In LoRa, Code Rate refers to the forward error correction code added to a packet before transmission. LoRa utilizes Hamming Code as the forward error correction code used in CR. The settings embedded into the chips are shown in Table 1. CR setting of 4/5 indicates that with every four bits of data, one bit of correction code will be added and subsequently CR4/8 refers to four bits of data with four additional correction bits. CR induces overhead to the transmission by increasing the number of bits to be transmitted. This overhead allows receiver to check for the correctness of the received chirps and provides a possibility to correct some erroneous bits from a chirp.



(a) Line-of-Sight. (b) Non-Line-of-Sight.

Fig. 5. Communication distance of each Spreading Factor on different environment. LoRa devices are still able to communicate beyond 9km for line-of-sight environment, however, LoRa signal propagation is severely impacted when obstructed.

Experiment Setup

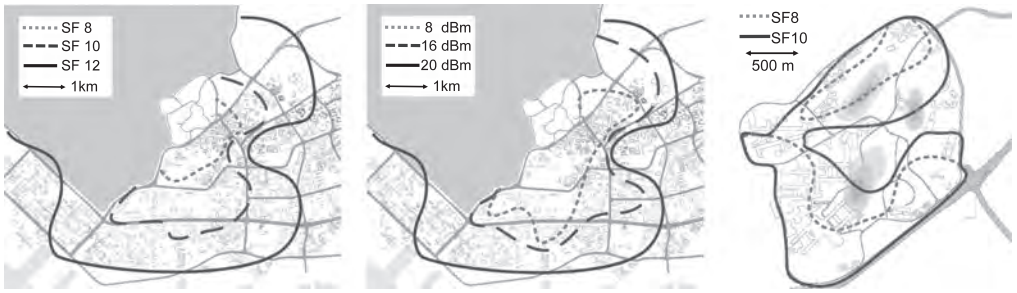
As Semtech gateway chipset allows changes of SF, TX Pow, CR on the fly but requires BW to be set to 125kHz, we conducted an experiment to measure the communication distance of each SF, TX Pow, and CR (excluding BW) and presents the highest packet reception rate (PRR) among the TX Pow and CR for each SF in Figure 5. With high number of buildings with heights ≥100m blocking line-of-sight (LoS) across Singapore and tallest buildings being private properties with restricted access to public, we performed the LoS experiment by the beach where LoS could be observed at all time with limited building in the vicinity. The packets with payload of 10 Bytes were transmitted by several end nodes across the 9.08km stretch while maintaining LoS at all times. Each node transmits equal number of packets for every combination of settings.

For the non-line-of-sight (NLoS) experiment, we performed the experiment on our campus grounds, which represents a metropolitan cityscape with high density of high-rise buildings (buildings height of ≥100m on average) blocking LoS between transmitter and receiver. The experiments were conducted on a 3×3km area with high density of high-rise structures and natural vegetations. In this experiment, end nodes transmit packets of different settings with payload of 10 Bytes continuously for ten minutes. Equal number of packets were sent for each setting from a single node. The end nodes were placed under open-air with no shelter. Buildings and trees would be present on test locations obscuring LoS without blocking the sky view.

To further test LoRa coverage, similar experiment was conducted for indoor and semi-indoor environment. Identical to the experiment done for the outdoor environment, each end nodes transmit for ten minutes period with payload of 10 Bytes and each setting will be transmitted equal number of times. However, three gateways were placed surrounding the 1×1km area were used to provide a better coverage within the area due to high attenuation caused by buildings. In this experiment, the indoor environment refers to end nodes being placed inside a building and within a room, while the semi-indoor environment refers to end nodes placed under a shelter that has access to open space, such as sheltered walkways and corridors by a building. Indoor and semi-indoor environments were combined to provide a view of LoRa coverage for deployment within and around a complex of buildings.

Line-of-Sight

The experiment results are presented in Figure 5(a). LoRa is capable of communicating up to 4 and 5km for PRR 90% and 70%, respectively, by using the fastest SF setting of SF7. However, the experiment was unable to uncover the maximum coverage of LoRa transmission beyond SF7.



(a) Outdoor coverage with TX Pow 20dBm and varying SF.

(b) Outdoor coverage with SF12 and varying TX Pow.

(c) Indoor coverage with TX Pow 20dBm and varying SF.

Fig. 6. LoRa coverage for different environments with PRR >70% and CR4/8. LoRa coverages are severely impacted on the east side of the map due to high density of buildings obstructing LoS.

Regression were performed on available data to extrapolate the PRR for distance beyond 9km. With the extrapolated data, LoRa is expected to be able to support up to 10km using SF12 with PRR 70%.

Outdoor Environment

Data presented in Figure 5(b) reveals that LoRa performance declined drastically in NLoS scenario for outdoor urban environment. In such complex environment, LoRa is only capable of covering the distance of 0.1 and 0.3km for PRR 90% and 70%, respectively, using SF7. Similarly, for SF12, <2km is the limit for PRR 70%. Moreover, similar to the studies presented in Reference [35], the results in Figure 6(a) indicates that LoRa transmission is heavily impacted by buildings. The transmission coverage was reduced significantly on the east part of the map as compared to the north and south parts. The west part of the map is inaccessible and thus unable to be explored for experiments. As compared to the line-of-sight coverage, the impact of the environment could reduce the coverage by 82% on average and around 90% for the worst case (east side of the map using SF12). This proves that LoRa signals are severely hampered by obstructions such as high-rise buildings. Furthermore, as seen in Figure 6(b), the benefit of increasing the TX Pow is limited and terrain dependent. The increase of transmission distance on sparse terrain could go up to 30% (16 to 20dBm on southwestern side of the map); however, the average gain in increasing TX Pow is <7%.

Indoor and Semi-Indoor Environment

Shown in Figure 6(c), the experiment was conducted only within the 2 × 2km area with the highest and lowest points being 77 and 8m, respectively. The results are confined within this area while coverage beyond this area has been covered in LoS and NLoS experiments. The coverage of lower SF (SF8 and SF10) forms islands due to obstructions of terrains and buildings blocking the direct paths resulting in high signal attenuation. However, SF12 is capable of covering the entire test area with little degradation.

Through a series of experiments, LoRa proves to be capable of communicating beyond what was claimed by Semtech in LoS environment. However, LoRa coverage degrades significantly with the presence of obstructions. For optimal coverage, system adopters would have to carefully choose the location for gateways and end nodes to ensure LoS. Where LoS is not attainable, system adopters would have to carefully choose the settings to ensure coverage while ensuring the lifetime of an end node.

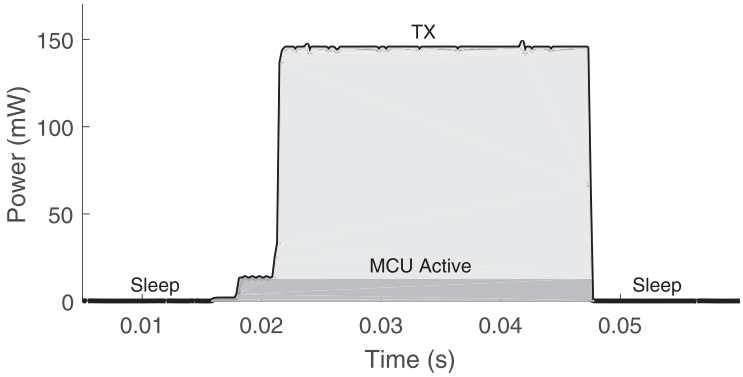


Fig. 7. Energy consumption captured by power monitor for a LoRa transmission with parameter SF7, CR4/5, 125kHz BW, 2dBm TX Pow, and 9 Bytes payload. Several states could be observed and dissected to model the energy consumption of a LoRa end node.

3.2 Lifetime of Nodes

This section conducts a group of experiments to capture the energy utilization of both the microcontroller (MCU) and LoRa transceiver of an end node under strategic conditions to explore useful information. These experiments are guided by a variance of SF, CR, TX Pow, and BW. Useful combinations of parameters were selected to conduct experiments for analyzing important aspects of energy consumption of both end nodes MCU and LoRa transceivers. First, we state the generic transmission energy profile of the end node for a single transmission. This energy profile is obtained using Monsoon Power Monitor and readings can be exported for further processing. Figure 7 illustrates the data exported from the power monitor. Energy consumption of a single transmission can be broken down to several components. These components can be grouped into *active* and *sleep* states. In *active* state, there are operating MCU, which requires energy to execute tasks and also Radio, which also require energy to transmit the packet. For *sleep* state, MCU still requires energy for time counting. Although small, the energy could take up to a considerable amount across a long period of time. Monsoon Power Monitor is used throughout this section to obtain ground truth of the hardware's energy profile.

The first experiment was conducted to compute the energy per transmission for all SFs ranging from SF7 to SF12 with a payload of 6 Bytes. Energy profile of the MCU and the transceiver were separately recorded for each transmission and is presented in Table 2. This experiment presents the two extremes in LoRa transmission configuration. The SF7 2dBm setting representing the least energy consuming configuration and the SF12 20dBm setting representing the most energy consuming parameter configuration. With 15 minutes interval between each packet, the experiment shows that LoRa nodes can sustain a lifetime of 4.60 and 1.37 years, respectively. These indicates that the 10 years end node lifetime promised by LoRa would be possible only through careful selection of parameter configuration and duty cycling.

The results in Table 2 can be calculated using Equation (2). The parameter T_{cycle} refers to the time duration of a single transmission cycle with duty cycle constraint. Energy parameters E_{batt} and E_{cycle} each refers to the energy contained in a particular battery and energy expended for each T_{cycle}, respectively. The lifetime calculated in Equation (2) assumes a perfect battery with no degradation due to time or environmental influences:

$$Lifetime = T_{cycle} \times \frac{E_{batt}}{E_{cycle}}. \tag{2}$$

Table 2. LoRa Packets Energy Budget Breakdown with PL = 6 Bytes, CR = 4/8, BW = 125kHz, 15min per Packet for SF7 and SF12, and Battery Capacity of 3.7V 2Ah

States		Time (ms)	Energy (mJ)	Budget (%)
SF7 2dBm	MCU Active	40.50	0.50	0.30
	MCU Sleep	899,959.50	71.28	43.14
	Radio TX	38.85	4.36	2.64
	Radio Sleep	899,961.15	89.10	53.92
		Total	165.24	4.60 years
SF12 20dBm	MCU Active	933.00	12.25	2.22
	MCU Sleep	899,067.00	71.21	12.87
	Radio TX	926.70	380.73	68.82
	Radio Sleep	899,071.30	89.01	16.09
		Total	553.20	1.37 years

Table 3. Energy Consumption for Different Type of MCU During a LoRa Packet Transmission

MCU	E_{MCU_On}	E_{MCU_Off}
Arduino Pro Mini	12.49mW	81.08μW
Arduino Uno	23.48mW	174.65μW
Raspberry Pi	1.41W	

We compute the time duration for a transmission cycle as a function of duty cycle in Equation (3). As duty cycle is the percentage of time a radio is transmitting, we compute the cycle duration T_{cycle} with $duty_cycle$ as the indication of a fraction of time the radio is allowed to transmit where T_{pkt} represents the transmission duration of a packet:

$$T_{cycle} = 100 \times \frac{T_{pkt}}{duty_cycle}. \tag{3}$$

The energy contained in a particular battery can be obtained through Equation (4) where the constant value of 3,600 refers to the number of seconds in an hour, C_{batt} refers to the charge in the battery with the unit of Ampere per hour (Ah), and V_{nom} as the nominal voltage of the battery:

$$E_{batt} = 3600 \times C_{batt} \times V_{nom}. \tag{4}$$

Recall in Figure 2 where LoRa PHY packet structure contains mandatory preamble of 2 symbols of sync word and 2.25 symbols of SFD, the transmission duration (T_{pkt}) can be calculated using Equation (5) with the number of preamble symbols defined by user (S_{pre}), number of payload symbol (S_{pl}), and T_{sym} defined in Equation (1):

$$T_{pkt} = T_{sym}(S_{pre} + 2 + 2.25 + S_{pl}). \tag{5}$$

To obtain E_{cycle}, on top of T_{pkt}, the energy expended by radio and MCU is required. These energy levels will have to be separated into two main states, *sleep* and *active/TX*.

Table 3 presents the energy consumption by MCU for both the *active* (E_{MCU_On}) and *sleep* (E_{MCU_Off}) states. The E_{cycle} mentioned in Equation (2) can be obtained through Equation (6)

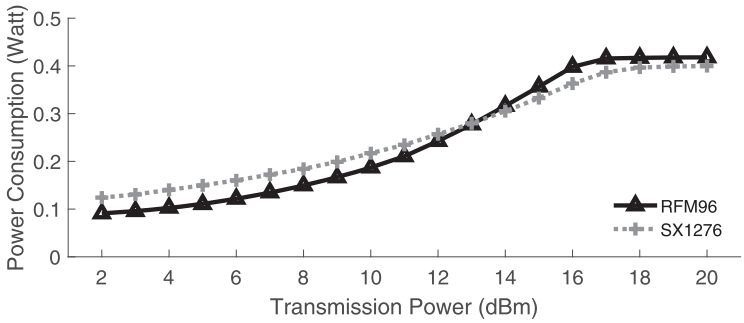


Fig. 8. E_{R_TX} of different TX Pow across all settings of SF, BW, and CR using Semtech *SX1276* and HopeRF *RFM96* chipsets. The two chipsets are relatively similar in their power profiles.

where E_{cycle} is divided into two parts, the energy expended during sleep state and energy expended during active state, which the duration is based on $T_{cycle} - T_{pkt}$ and T_{pkt}, respectively. The energy expended during sleep state requires the information of E_{MCU_Off} and also energy expended by Radio during sleep E_{R_Off} while the energy expended during transmission would require the information of E_{MCU_On} and energy expended by Radio during transmission E_{R_TX}:

$$E_{cycle} = [(T_{cycle} - T_{pkt})(E_{MCU_Off} + E_{R_Off})] + [T_{pkt}(E_{R_TX} + E_{MCU_On})]. \tag{6}$$

Semtech datasheet provides Equation (7) to calculate S_{pl}. The variables in the equation are Payload in bytes (PL), SF, CR, IH as 0 or 1 to indicate explicit or implicit header, respectively, and both CRC and DE as 0 or 1 to indicate absence or presence as required. DE is recommended to be set to 1 if T_{sym} exceeds 16ms:

$$S_{pl} = 8 + max\left(4CR\left\lceil\frac{8PL - 4SF + 28 + 16CRC - 20IH}{4(SF - 2DE)}\right\rceil, 0\right). \tag{7}$$

To predict E_{R_TX}, we conduct exhaustive tests for all settings that includes SF, BW, CR, TX Power on Arduino Pro Mini with *SX1276* (on inAir9B) and *RFM96* chipsets. The experiment resulted in >12GByte of measurement data.

We extract the energy consumed by each measurement by converting the energy reading to the scale of Joule per second (Watt). The energy consumption is further grouped by chipsets and TX Pow. The values are then averaged and presented in Figure 8. We compute a cosine similarity for the power profile of both chipsets and obtained a similarity value of 0.994.

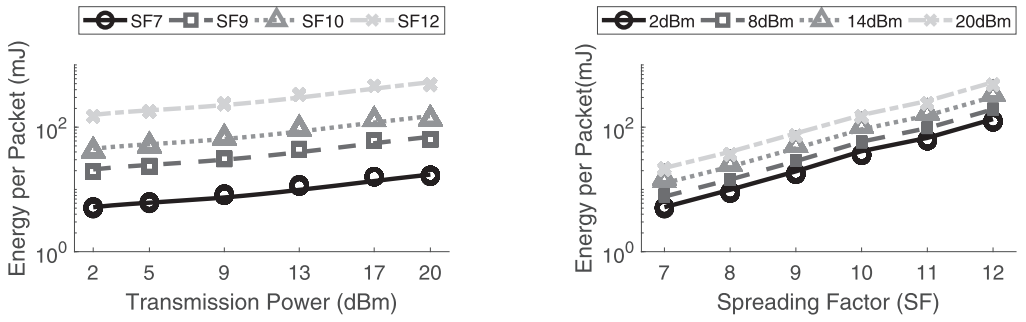
Based on the results in Figure 8, a polynomial function presented in Equation (8) can be obtained through regression. We select degree (d) 12 and 10 for *SX1276*[1] and *RFM96*[2] chipsets, respectively, for optimal performance:

$$E_{R_TX} = \sum_{n=0}^{d} \alpha_n x^n. \tag{8}$$

The results of our prediction model is shown in Figure 9 where each marker represents actual measured data for the particular settings and the line represents the output of prediction model. The energy consumption prediction model achieved a mean error of 0.30% for both chipsets.

[1] R_{TX} coefficients for SX1276 chipset: α_0 = −1.860e-01, α_1 = 6.258e-01, α_2 = −5.478e-01, α_3 = 2.724e-01, α_4 = −8.534e-02, α_5 = 1.788e-02, α_6 = −2.584e-03, α_7 = 2.609e-04, α_8 = −1.833e-05, α_9 = 8.779e-07, α_{10} = −2.726e-08, α_{11} = 4.951e-10, α_{12} = −3.980e-12.

[2] R_{TX} coefficients for RFM96 chipsets: α_0 = −3.523e-01, α_1 = 7.024e-01, α_2 = −4.630e-01, α_3 = 1.680e-01, α_4 = −3.724e-02, α_5 = 5.315e-03, α_6 = −4.976e-04, α_7 = 3.033e-05, α_8 = −1.157e-06, α_9 = 2.501e-08, α_{10} = −2.3351e-10.



(a) Varying TX Pow.

(b) Varying SF.

Fig. 9. Measured and predicted energy consumption with varying settings represented by markers and lines, respectively. The model is able to predict the energy consumption of different settings with minimum deviation.

Table 4. Predicted Nodes Lifetime and Expected Error Under Specific Settings and Hardware on a 2Ah Battery

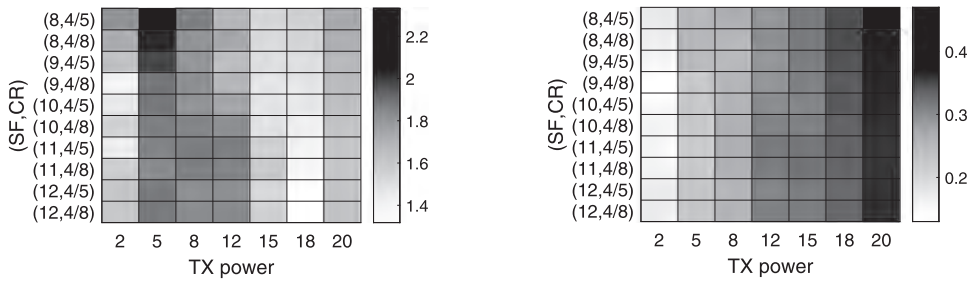
Settings	ProMini + RFM96	ProMini + SX1276	Uno + RFM96	Uno + SX1276
SF7, CR4/5 125kHz, 10dBm payload 10 Bytes 0.01% duty cycle	4.54 years ±5 days	3.87 years ±4 days	3.01 years ±3 days	2.70 years ±3 days
SF9 ,CR4/7 125kHz, 14dBm payload 18 Bytes 0.1% duty cycle	1.71 years ±2 days	1.65 years ±2 days	1.41 years ±2 days	1.37 years ±2 days
SF12, CR4/8 125kHz, 14dBm payload 24 Bytes 0.1% duty cycle	1.42 years ±3 days	1.39 years ±2 days	1.21 years ±2 days	1.19 years ±2 days

A careful selection of MCU could drastically affect the lifetime of end nodes.

We present Table 4 to demonstrate the influence of hardware and setting selections on the lifetime of the end nodes. As expected, duty cycle is the major factor that determines the lifetime of nodes as the sleep state greatly reduces the energy consumption and allows longer lifetime. SF and TX Pow also play a large part in the lifetime of end nodes as these settings will determine the time duration of a packet and the amount of energy to be used for the transmission.

Figure 10 shows the prediction error of the prediction model for both E_{R_TX} and energy expended by E_{cycle} with T_{cycle} of 15min. Although there is more error for the lower TX Pow settings in Figure 10(a), the error is not reflected for the same setting in Figure 10(b). This is accredited to the long duration of the sleep state, which contributes to the increase of the proportion for E_{MCU_Off} and E_{R_Off} in the E_{cycle} and dwarfs the prediction error of E_{R_TX}. However, Figure 10(b) shows the prediction error worsen as TX Pow increases. This is due to the hardware variation as the prediction model inputs are the averaged readings of the energy expended across multiple hardware.

Figure 11 presents the CDF of prediction error as compared to ground truth. The model yields a 3.08% error at the 90th percentile and 1.66% error at the 50th percentile. As the model only predicts E_{R_TX}, researchers and system adopters would be able to easily compute E_{cycle} by substituting



(a) E_{R_TX} (b) E_{cycle}

Fig. 10. Prediction error for E_{R_TX} and energy consumption of MCU + Radio scenario for 15min inter-packet delay compared to measured readings. By Including MCUs energy consumption, prediction errors of E_{R_TX} become insignificant.

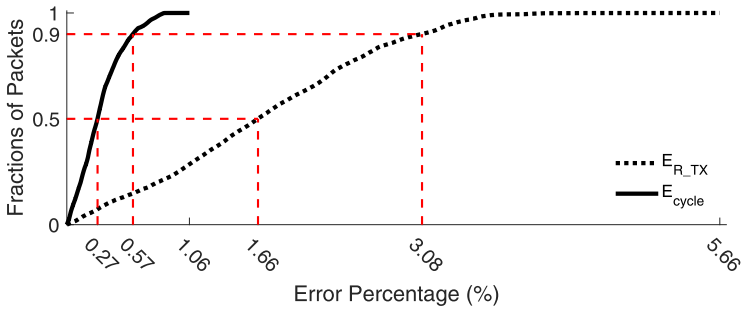


Fig. 11. CDF of the prediction error per cycle for combinations of *SX1276* and *RFM96* chipsets with Arduino Uno and Arduino Pro Mini. Regardless of the type of chipsets, prediction errors are still below 6% and with MCUs energy consumption, prediction errors drops to a little over 1%.

E_{MCU_Off}, E_{MCU_On}, and E_{R_Off} to predict a node energy consumption and lifetime with other type of MCUs.

3.3 Multiple Access

This section characterizes LoRa's Multiple Access performance through a series of experiments. In contrast to common LPWAN protocols such as Sigfox [54], WiFi HaLow [3], LTE-M [1], and Weightless [64], a fundamental difference in LoRa modulation is its capability to perform concurrent communications within a single physical channel. This provides LoRa networks a significant advantage under dense environmental conditions.

This concurrency is due to two factors. First, a standard LoRa gateway receives simultaneous transmissions from multiple physical channels. Second, it also efficiently differentiates between simultaneous orthogonal transmissions, even if such transmissions are within the same physical channel. In contrast to the capabilities of end nodes based on the SX127X LoRa transceivers, a standard LoRa gateway gains this extra performance at the cost of increased processing power, additional hardware, cost, space and power. Figure 12 presents an abstract baseband block diagram of a standard LoRa gateway, namely, the IMST IC880A concentrator. The IMST IC880A gateway design incorporates a single SX1301 LoRa baseband signal processor and two full-duplex SX1257 RF front-end to digital IQ modulator/demodulators. To adhere to the LoRaWAN standard, which mandates several physical channels based on the ISM band, both front end ICs collaboratively share the bandwidth. The SX1301 continuously processes two simultaneous IQ streams from the

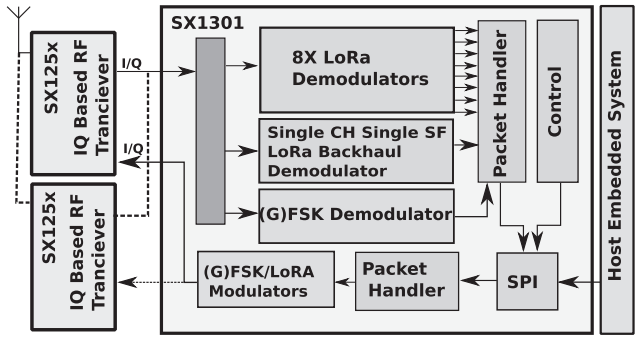


Fig. 12. Block-level overview of a LoRa SX1301 concentrator.

SX1257 ICs and interprets IQ data in accordance with the LoRa PHY. The decoded information is later made accessible to a host via the SPI protocol.

The SX1301 integrates the LoRa IP and supports 10 configurable receiving channels. These 10 falls under three categories based on their use cases and programmability. Eight of them are by design fixed in BW to 125KHz, while the channel frequencies of those are programmable. They are by design expected to be used to receive packets from end nodes. Out of the remaining two, one is connected to a GFSK demodulator while the other to a functionally limited LoRa demodulator designed to be used as a backhaul channel to other gateways or infrastructure. The limitation on the backhaul LoRa channel is that it only operates on a single SF of choice as opposed to the aforementioned 8 LoRa channels, which demodulate any given SF. However, the backhaul channel has the advantage of operating on 125, 250, or 500KHz of channel BW.

Semtech asserts that a SX1301-based gateway is able to simultaneously demodulate a maximum of eight concurrent packets [59] as long as non-orthogonal transmissions are separated to different channels. Orthogonal transmissions are a key feature in a LoRa modulation that diversify spectrum usage and minimize collisions. They are further explained under Section 4. Given this resiliency to orthogonal transmissions, an estimate of concurrent reception capability at the gateway directly translates to an indicator that reflects LoRa's multiple access capability. We leverage this to estimate LoRa's multiple access capability through a series of experiments.

Capacity of LoRa Spreading Factors

The experiment setup consisted of 50 randomly placed SX1276-based nodes with payload of 10 Bytes and a single IMST IC880A gateway. The 50 nodes were used to emulate a higher number of nodes based on their duty cycle. The emulation assumed that a typical LoRaWAN node adheres a duty cycle of 0.1% as a viable duty cycle enlisted in the LoRaWAN specification. Therefore, a node that transmitted at a duty cycle of 1% was considered to emulate 10 nodes, and so on.

First, we performed a test to determine the performance of LoRa's individual SFs. To do so, all nodes were programmed to randomly transmit packets of same SF for a duration 15min. The duty cycle of real-nodes was controlled to emulate up to 12,000 nodes in steps of 100 under different experiment iterations. For each iteration, the PRR and throughput were computed. Figure 13 depicts the results of this experiment for selected PRRs of 90%, 80%, 70%, and 50%. Based on our results, we also computed the impact on PRR with increasing number of transmitted packets during the period of 15min. We present this result in Figure 14 for all SFs.

Although the airtime of SF7 is lowest for a given payload, one may assume that SF7 should in turn support the largest number of network capacity. However, the result indicated in Figure 13 suggests otherwise. It indicates that SF7 supports the least network capacity and SF12 the highest.

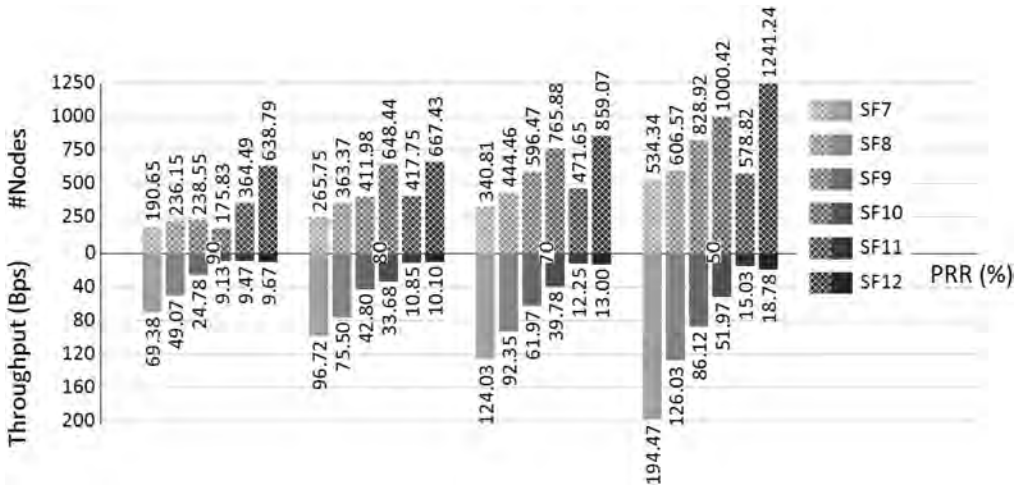


Fig. 13. Single-channel capacity of a SF. Higher SF proves to support more nodes as packet collision reduces as compared to lower SF, however, the low throughput of higher SF on contrary to the higher nodes supported is due to the lower number of packets transmitted.

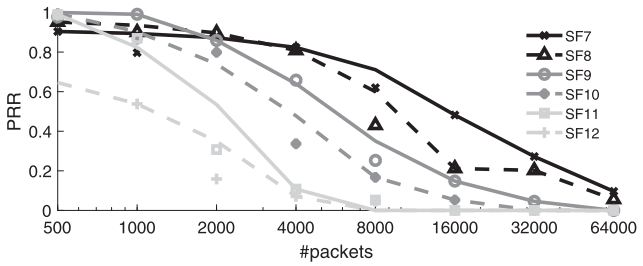


Fig. 14. PRR of each SF for increasing transmission. The PRR decreses as the number of packets transmitted increases which provides a hint in explaining the phenomena observed in Figure 13.

The reason for this observation, although counterintuitive, is due to the permitted airtime of the nodes based on the duty cycle of 0.1%. To elaborate, in comparison to an SF12 end node, an SF7-based end node is allowed to transmit a higher number of packets as the airtime consumed by same payload is significantly lower. Effectively, an SF12-based network is permitted to transmit significantly less number of packets than a SF7-based network.

The higher number of packets from SF7 end nodes increase the chances of packet loss as a large number of non-orthogonal transmissions use the same physical channel. This in turn limits the concurrent demodulation capability at the gateway. With increased collisions, the number of correctly received packets at the gateway is reduced. Therefore, the number of supported nodes is also reduced. By extension, a SF12 setting supports more nodes achieving a higher network capacity under the same duty cycle. In addition, SF7 achieves multiple orders of higher throughput in comparison to a SF12-based network due to the higher numbers of packets transmitted. This is observed in Figure 13.

Capacity of a Single LoRa Channel

In this experiment, we evaluate the capacity of a single LoRa channel as well as the extent of concurrent demodulation capability of a LoRa gateway under three different ratios of SFs. Testing

Table 5. Experiment Settings for Single-channel Performance

Parameter	SF7	SF8	SF9	SF10	SF11	SF12
$\beta = 12$	50.79%	25.40%	12.70%	6.35%	3.17%	1.59%
$\beta = SF$	16.67%	16.67%	16.67%	16.67%	16.67%	16.67%
$\beta = 7$	1.59%	3.17%	6.35%	12.07%	25.40%	50.79%

An end node in an indoor environment ($\beta = 12$) will have a higher chance to transmit in SF7, resulting in a higher number of SF7 packets and vice versa.

the decoding capability of the concentrator based on the performance of individual SFs is not a true indicator of the overall performance, because a typical LoRa environment contains packets from a range of SFs that arrive at the concentrator. Therefore, a more meaningful method of validating multiple access performance of a single LoRa gateway would be to test its performance under commonly available environmental conditions:

$$f(\beta, SF) = 2^{|sf-\beta|}. \tag{9}$$

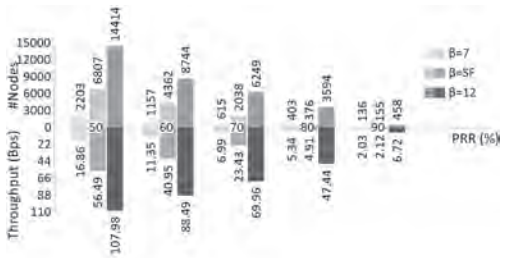
The choice for a SF is mostly motivated by the distance and energy budget in typical LoRa-based applications. For the sake of simplicity, we consider that these applications fall within the three environments namely, indoor, semi-indoor, and outdoor. We assume that an indoor environment consists more nodes that transmit using lower SFs and vice-versa for an outdoor environment. We also assume that a semi-indoor environment consists of nodes with a balanced ratio from all SFs. Having defined the three environments, we now parametrize them in Equation (9). Three values for β in Equation (9) are strategically chosen such that the results represent the percentage of nodes for each SF for a fixed value of β, i.e., a set environment. In this case, $\beta = 7$ signifies an outdoor network, $\beta = 12$ an indoor network while $\beta = SF$ signifies a semi-indoor network. For further clarity, we present these ratios in Table 5.

The setup for this experiment is as follows. First, all randomly placed nodes with a payload of 10 Bytes were assigned a spreading factor based on the SF ratio for a single β value representing a particular environment through Equation (9). In contrast to the previous experiment, this experiment achieved the emulation of nodes differently. Here, we assumed a network of LoRa nodes that transmitted every 15min. Therefore, a node that transmitted 100 times within 15min emulated 100 LoRa nodes, and so on. Last, the aforementioned process was repeated for the remaining two β values.

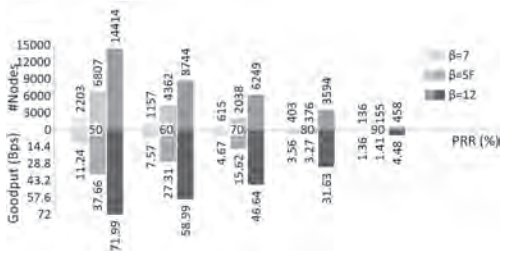
The results were then processed to determine the number of nodes that can be supported under PRRs ranging from 50%, 60%, 70%, 80%, and 90% along with respective throughput and goodput rates as presented in Figure 15.

The results of the experiment indicate that an indoor environment ($\beta = 12$) supports the highest throughput and PRR settings. This result is intuitive as node density is solely determined by the number of transmissions under 15min. In other words, as transmissions that consume less airtime are present in the environment, more throughput and a higher number of nodes can be supported for the same PRR. Finally, to better present the gateway's decoding capability, we also present Figure 16, which depicts a snapshot of the decoding progress of the gateway while 10 nodes randomly transmitted packets using different SF.

On the contrary, results in Figure 15 seemingly disagrees with those in Figure 13. The results from our previous experiment that concluded the capacity of SFs favored SF12 nodes. However, in this experiment, we observed that a higher number of SF7 nodes correspond to an increase in the total supported nodes. While the results seem contradicting, the latter experiment utilized a ratio of different SFs whereas the former utilized a single SF. Recall the condition for concurrent



(a) number of nodes and throughput supported by a single LoRa channel for varying PRR.



(b) number of nodes and goodput supported by a single LoRa channel for varying PRR.

Fig. 15. Capacity of a single LoRa channel under multiple β settings. Number of nodes supported, throughput, and goodput increases along with the increase of SF7 packets.

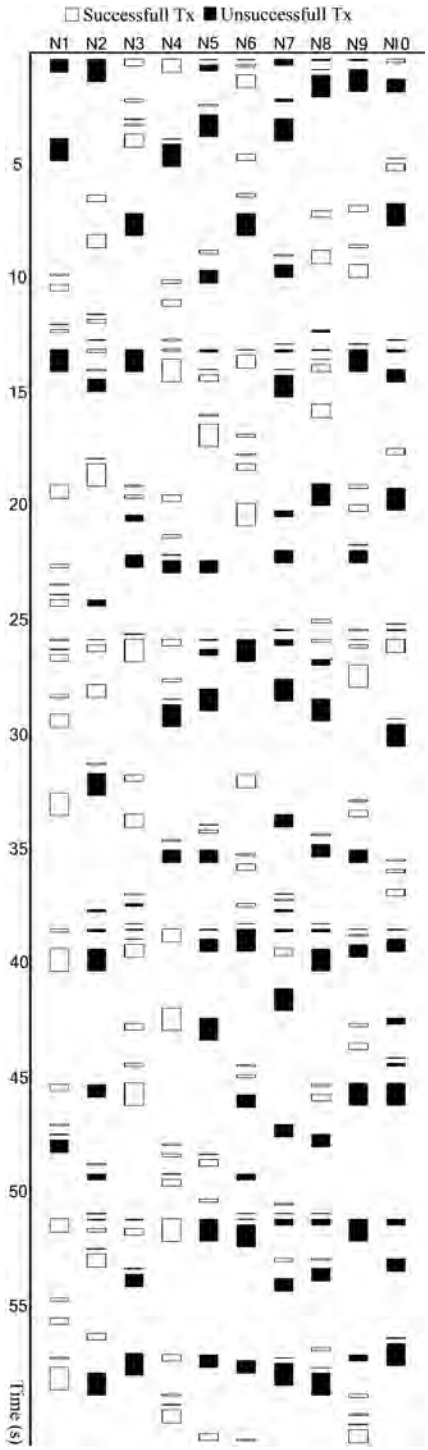
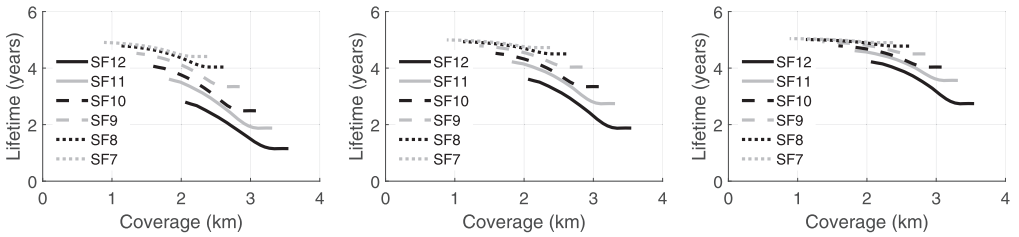


Fig. 16. Emulated traffic from 2,000 nodes received by gateway with $\beta = SF$.



(a) Inter-packet delay of 15 minutes.

(b) Inter-packet delay of 30 minutes.

(c) Inter-packet delay of 60 minutes.

Fig. 17. Lifetime and coverage of all settings for PRR of 0.7 in NLoS environment. The skyline of all curves in each figure is the optimal settings for the given inter-packet delay.

demodulation of a gateway. The multiple SFs utilized in the latter experiment enhanced the concurrent decoding capability of the gateway while the former suppressed the same. Having a ratio of SFs provides an opportunity to the gateway to demodulate multiple packets resulting in a higher throughput and an increase in the number of supported nodes. However, SF12, having the highest airtime, becomes detrimental as colliding packets of same SF are not received correctly within the same channel.

The experiments in this section were performed to quantify the performance in of single physical channel. A study across multiple channels is required to fully understand the network capacity of a single gateway LoRa network, since LoRa concentrator chipset promises concurrent demodulations across channels.

4 BEYOND LORA

This section reports our studies beyond LoRa practices and provides insights through an SDR-based LoRa PHY analysis. We also report optimization and improvement opportunities to existing LoRa practices.

4.1 Parameter Optimization for Communication Distance

This section proposes an algorithm to search for the optimized parameter setting for a given communication distance and a node lifetime restriction. Based on the results in Sections 3.1 and 3.2, which predict the communication distance and lifetime of a node, respectively, for any given parameter settings, the proposed Algorithm 1 makes use of the prediction model $f_{coverage}()$ and $f_{lifetime}()$, which are derived using transmission distance and node lifetime in years as a function of SF and TX Pow. The models make use of experimental data, which are first filtered by using PRR threshold to remove any data points below the given PRR. Filtered data are then used in the polynomial regression to train the models. Since the input of both models are similar, a simple search through the SF and TX Pow combination is used and all settings that fulfill the requirement of $f_{coverage}()$ are then used as input to $f_{lifetime}()$.

The resulting output from $f_{coverage}()$ and $f_{lifetime}()$ is presented in Figure 17 where different inter-packet delays are used for the three figures. Each setting's coverage is plotted against its respective lifetime with TX Pow increasing along the x-axis. These figures are generated based on the profile of a LoRa node transmitting 10 bytes of payload with eight preamble symbols and code rate of CR4/8. The inter-packet delays are 15, 30, and 60min, respectively.

According to the results in Figure 17, SF could reach further distance but TX Pow would provide better lifetime. As observed in the figures, lower SF with higher TX Pow provides similar coverage but with longer lifetime. A simple optimization to the algorithm can be applied by making use

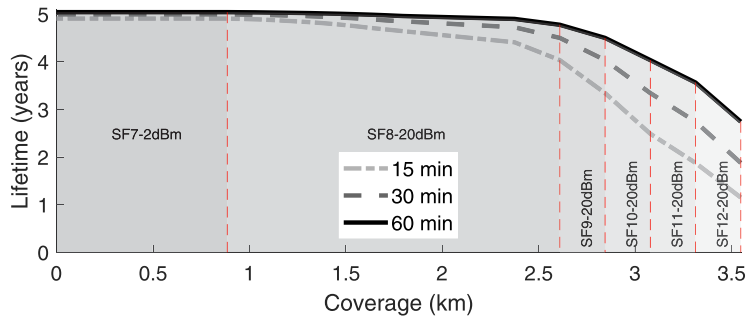


Fig. 18. Setting selections for optimal coverage and lifetime. Exhausting TX Pow before SF would results in a node with better coverage and longer lifetime.

ALGORITHM 1: An optimal settings searching algorithm.

Input:

Th_d: Threshold for minimum required distance
Th_{lf}: Threshold for minimum required node lifetime
T_{cycle}: Packet interval requirement
$f_{coverage}()$: Prediction model for LoRa coverage
$f_{lifetime}()$: Prediction model for LoRa lifetime

Output:

$S_{optimal}$: A set of optimal settings (sf, tx_pow)

Initialize:

$S_{optimal} \longleftarrow \{\}$

1: **for** $sf \in \{SF12, \ldots, SF7\}, tx_pow \in \{20dBm, \ldots, 2dBm\}$ **do**
2: **if** $f_{coverage}(sf, tx_pow) \geq Th_d$ **then**
3: **if** $f_{lifetime}(sf, tx_pow, T_{cycle}) \geq Th_{lf}$ **then**
4: $S_{optimal} \longleftarrow (sf, tx_pow)$ ▷ settings fulfill conditions
5: **end if**
6: **else**
7: break ▷ skip remaining settings
8: **end if**
9: **end for**
10: **return** $S_{optimal}$

of the nature of SF and TX Pow, whereas SF and TX Pow increases, the coverage increases while lifetime decreases accordingly. This nature can be incorporated into the algorithm by searching through decrementing loops instead of incrementing loops. The algorithm only terminates the search while searching through the $f_{coverage}()$ but not $f_{lifetime}()$. This is mainly because the input of $f_{lifetime}()$ is a subset of the search space and early termination would not return the skyline of Figure 17, since many higher SF settings would have lower lifetime than the lower SF settings counterparts. Recall that the search is done using a decrementing search where higher SF and TX Pow values will precede the lower values.

We present the output of Algorithm 1 in Figure 18, which represents the optimal settings with given lifetime and coverage requirements. Observe that lifetime of a node is severely impacted by packet frequencies. However, the relationship of node lifetime and packet frequencies are

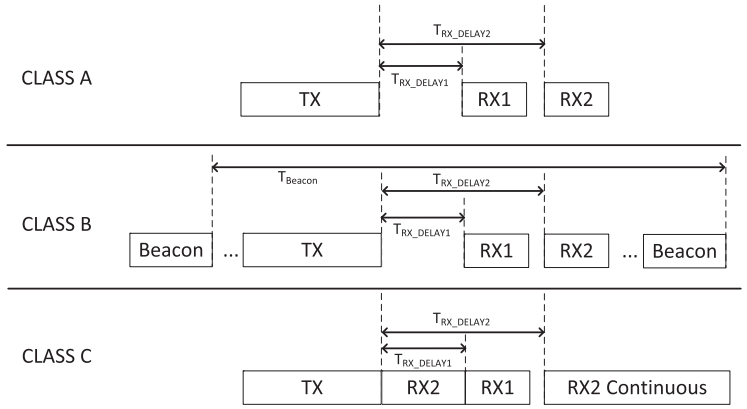


Fig. 19. Classes of LoRaWAN exhibit different network utilization behaviors.

non-linear. This is due to the power consumed during a node's sleep time, which is small but not negligible as sleep time increases.

The experiment results presented here provide a rule of thumb to system adopters and researchers. Since increasing SF results in lower lifetimes with higher coverage, SF should always be the last setting to be increased. System adopters would be able shorten the time to obtain optimal settings using the algorithm provided and researchers would be able to design more efficient setting adaptation mechanisms by considering the findings highlighted above.

4.2 Implication of LoRaWAN

This section discusses the LoRaWAN Medium Access Control (MAC) protocol, which serves as the guideline for LoRa's MAC layer as well as upper network stacks layers and the implication of LoRaWAN toward the performance of LoRa.

LoRaWAN proposes three types of classes to cater to different application requirements. Illustrated in Figure 19, the three classes are class A (All end nodes), B (Beacon), C (Continuous listening) [31]. Class A is the basic option that all LoRaWAN compliance end nodes should be able to support, while classes B and C are mutually exclusive additional features on top of class A. This implies that class C end nodes should not implement class B and vice versa.

Class A devices implement a node-initiated transmission where all downlink communication from the server to end nodes have to be initiated by an uplink transmission from end node to server. To enhance the reception of downlink communication, end nodes are required to schedule two reception slots after the initial transmission. The first reception slot uses the exact settings as prior transmission while the second reception slot uses a preprogrammed SF. First and second reception slots are initiated following a transmission after a T_{RX_DELAY1} and T_{RX_DELAY2}, respectively. These reception slots only act as a preamble detection window. In any case, where the packet in first reception window is designated for the end nodes, the second reception window would not be opened. Similarly, if the first reception window duration exceeds T_{RX_DELAY2}, the second reception window will also be aborted. LoRaWAN suggests five T_{sym} as timeout for each reception window.

As the name suggests, class B incorporate beacons to improve responsiveness of end devices. End nodes are expected to obtain T_{Beacon} from gateways and wakes up every T_{Beacon} to synchronize itself with gateways to open a short reception window when necessary. These reception windows will allow gateways to transmit any command from the server to end nodes within a T_{Beacon}.

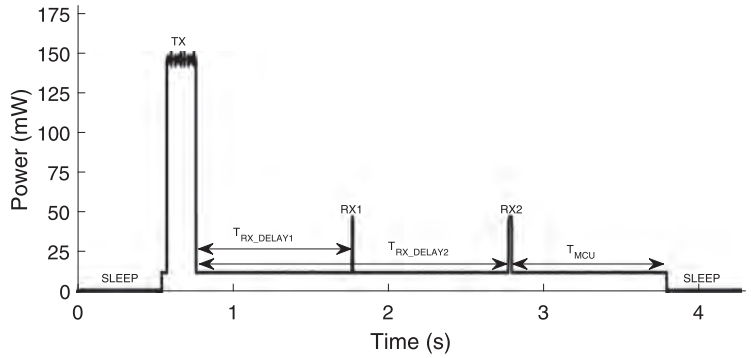


Fig. 20. Node energy consumption for a LoRaWAN transmission cycle. On top of the energy consumption due to RX, MCU has to stay awake throughout T_{RX_DELAY1} and T_{RX_DELAY2}, which increases the MCU energy consumption.

Class C is designed for real time applications that require immediate response from end nodes. With this class, end nodes are required to open a continuous reception window using the preprogrammed SF. Instead of waiting for T_{RX_DELAY1} before reception, class C devices immediately open a reception window with preprogrammed SF for T_{RX_DELAY1}. After T_{RX_DELAY1}, end nodes switches the reception settings to settings used in transmission before going back to preprogrammed settings after T_{RX_DELAY2}.

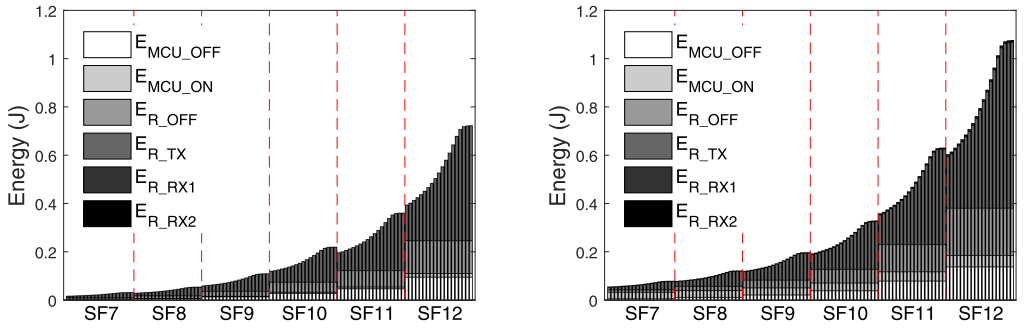
LoRaWAN incorporates additional overhead into the packet to enable the Medium Access Control (MAC) features provided by classes above. These overheads include MAC headers, commands, and Message Integrity Checks (MIC). By combining the overheads, LoRaWAN imposes 13 to 27 Bytes of overhead onto each packet transmitted by an end node.

Energy Consumption

With the increase in packet size due to the MAC overhead and mandatory reception windows, energy consumption of an end node would increase accordingly. An energy consumption snapshot of class A end node is illustrated in Figure 20. Apart from the TX phase, there are two RX phases separated by predefined delays. Note that the MCU is not in low-power mode during the delays. These MCU active times would result in degradation of an end node's lifetime.

An experiment was conducted to explore the energy budget overhead of LoRaWAN as compared to LoRa. The experiment measures energy consumption of a transmission cycle, which includes both active and sleep time of an end node. Energy consumption of end nodes was measured using Monsoon power monitor and payload size was set to 10 Bytes with 0.1% duty cycle to adhere to LoRaWAN standards. For each packet, CR is set to CR4/8 and 100 packets were transmitted for each SF and TX Pow setting combination. For LoRaWAN packets, we assume no downlink traffic from gateway, which requires end nodes to execute both RX windows with default RX timeout of five symbol time. Energy consumption are first grouped according to the settings followed by grouping of energy consumption according to component states (E_{MCU_OFF}, E_{MCU_ON}, E_{R_OFF}, E_{R_TX}, E_{R_RX1}, and E_{R_RX2}). After grouping, each group are then averaged to obtain the energy consumption of each states for each setting. Experiment results are presented in Figure 21.

Results show that LoRaWAN imposes 149% to 313% overhead on energy consumption as compared to LoRa with average of 198% times increment across all settings. This increment is due to the increase in MCU active time while waiting for RX windows mandatory in LoRaWAN standard. However, note that with acknowledgment (ACK) packets from gateway, such overhead could be



(a) LoRa . (b) LoRaWAN .

Fig. 21. Energy budget required by a transmission cycle for packet with payload of 10 Bytes and 0.1% duty cycle with varying SF and TX Pow. LoRaWAN energy budget for E_{MCU_OFF} and E_{MCU_ON} is significantly higher than the LoRa counterparts.

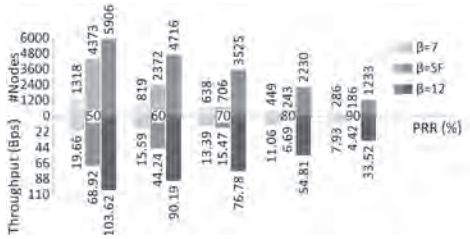
reduced as end nodes are expected to not start the second RX window if ACK or downlink packets are received in the first RX window. However, any long downlink packet could significantly increase the energy overhead.

Multiple Access

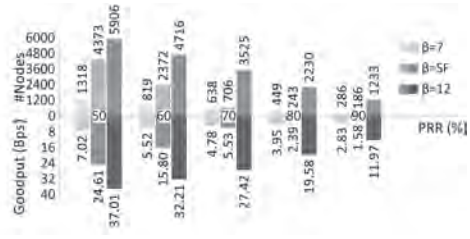
On top of the overhead in energy consumption, a MAC protocol also imposes limitations on packet transmission. This limitation affects several network parameters, which includes network density, throughput, and goodput. Since LoRa networks are expected to form a single-hop network without intermediate end nodes as relay, LoRa network density directly equates to number of end nodes supported by a gateway. This value could vary depending on the PRR requirement of said network. Similarly, throughput and goodput, which refers to the end-to-end number of bytes received and number of effective bytes received, respectively, also varies depending on PRR but are unaffected by multi-hop.

To investigate the effect of LoRaWAN-imposed limitation on parameters mentioned above, experiments were conducted using a SX1301 gateway concentrator with 50 end nodes equipped with SX1276 chipset. Similar to the experiment in Section 3.3, 50 nodes were used to emulates multiple nodes by manipulating the inter-packet delay. We first assume a standard transmission with inter-packet delay of 15min regardless of SF, then by halving the inter-packet delay, number of active nodes increase to 100. Using said method, number of emulated nodes transmitting in 15min could reach up to 500,000 nodes. Next, Equation (9) was used to vary the probability of a node in choosing a particular SF for transmission to simulate outdoor, semi-indoor, and indoor environment. Furthermore, to ensure no interruption due to ACK queuing and self-interference from ACK packets, downlink traffic was disabled. However, by disabling downlink traffic, end nodes were expected to activate both RX windows. TX Pow of the nodes are set to the maximum value of 20dBm, while CR are set to CR4/8. Payload size of each packets are set to 10 Bytes to aid comparing with results in Section 3.3.

Experiment results in Figure 22 show a significant advantage of more SF7 packets in the network as compared to equal chances, which signifies indoor and semi-indoor, respectively. Moreover, having many SF12 in the network could cause congestion and lower network performance. Comparing throughput and goodput of LoRaWAN system reveals that LoRaWAN packet overhead accounts to >64% of the traffic; however, this overhead would reduce as the payload size increases.

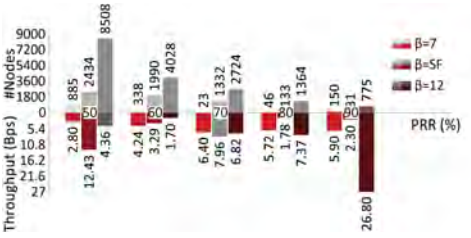


(a) Number of nodes and throughput supported by each PRR requirement.

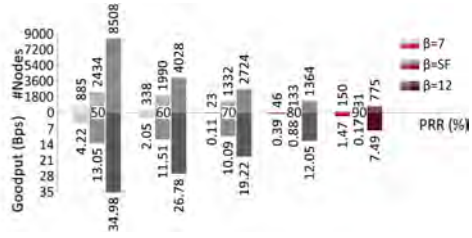


(b) Number of nodes and goodput supported by each PRR requirement.

Fig. 22. Comparison of throughput and goodput of a single gateway with LoRaWAN and supported number of nodes for each PRR requirement. Similar to results in Section 3.3, higher number of SF7 packets increases throughput, goodput, and number of supported nodes.



(a) Difference between LoRa and LoRaWAN in supported number of nodes and throughput for each PRR requirement.



(b) Difference between LoRa and LoRaWAN in supported number of nodes and goodput for each PRR requirement.

Fig. 23. Comparison of the difference in throughput and goodput of a single gateway between LoRa and LoRaWAN with supported number of nodes for each PRR requirement. Difference is computed as $\delta_x = LoRaWAN^x_{prr} - LoRa^x_{prr}$, where x refers to the number of nodes, throughput, or goodput. Hence, positive and negative δ_x are represented in the figure with red and gray bars, respectively. LoRaWAN packet overhead diminishes the benefit it brings.

LoRaWAN, which is the MAC protocol of LoRa, serves to organize the channel access behaviour of nodes within the network. This mechanism should provide certain degree of improvement over LoRa's disorganized behaviours. A comparison between the results of LoRa and LoRaWAN, which are presented in Figure 23, indicates that although in most cases LoRaWAN provides a higher throughput, the header overhead of LoRaWAN takes up most of the throughput. When observing goodput, which is throughput without the overhead, the benefit reported in throughput vanishes, leaving behind a much lower goodput compared to aloha LoRa. The high throughput reported was mainly due to the mandatory RX windows. These RX windows provide a chance for other nodes to make use of a clear channel to transmit packets. However, the same would not be true when downlink traffic is not disabled. Downlink traffics, especially ACK packets could block a significant amount of uplink traffics, since to transmit an ACK packet, gateway has to switch one of its two radio chains from RX mode to TX mode. This change in modes would disable all uplink traffics transmitting in the channels served by that particular radio chain within the period of time the ACK is transmitted. Moreover, a tight scheduling is essential to ensure minimal delay in de-queuing received packets and queuing ACKs. To offload the burden of a gateway in providing ACKs, all ACKs requests would be served by backend servers.

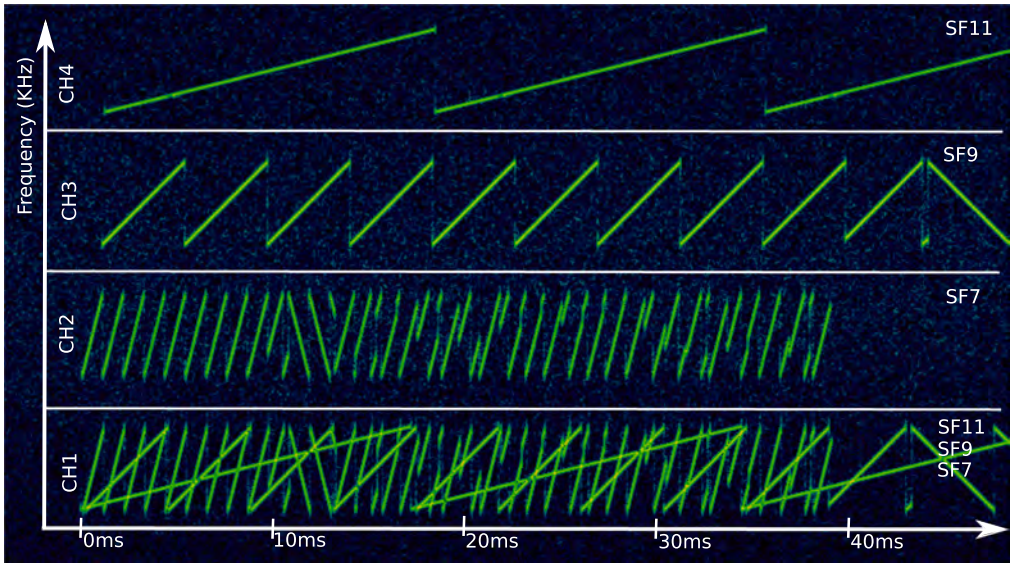


Fig. 24. Concurrent transmission of LoRa.

With the unique capability of LoRa gateway, which allows concurrent demodulation, an efficient MAC protocol is required, which takes into consideration of providing high packet reception rate with minimal ACKs and retransmission.

4.3 LoRa Medium Access

LoRa's physical layer is aloha in nature and incorporates no collision avoidance mechanisms. However, lost transmissions are undesirable within sensor networks and incur unbearable costs upon energy restricted nodes. In LoRa, only packets of same SF within a common channel are susceptible to disruptive collisions and the probability of such collisions increases with increasing network density. Traditional RSSI-based methods used for collision avoidance are ineffective on LoRa for two reasons. (1) Due to inherent properties from CSS modulation, successful LoRa transmissions may traverse below noise floor. (2) RSSI itself offers no capability to differentiate between single-channel concurrent transmissions. In this section, we focus on the performance of a LoRa concentrator in receiving orthogonal and non-orthogonal transmissions within single and multiple channels through a series of experiments. Based on their observations, we then propose a potential collision avoidance mechanism for LoRa, named CSMA-CAD, which improves PRR under dense network conditions.

Concurrent Reception Capacity of the LoRa Concentrator

LoRa's concurrency is highly reliant on orthogonal transmissions. Therefore, prior to discussing concurrency, we first illustrate orthogonal LoRa transmissions in the physical layer. To do this, we transmit three concurrent packets using distinct Spreading Factors SF7, SF9, SF11 within a single channel. At the same time, to better illustrate the chirps, we also concurrently transmit the same data on three different channels. We then capture this concurrent transmission using the SDR setup described in Section 2. Figure 24 presents a spectrogram of these LoRa transmissions. All channels were of 125KHz of BW. While CH2, CH3, and CH4 have only a single transmitting

Table 6. PRRs Under Varying Concurrent Conditions

#Concurrent Tx	2	3	4	5	6	7	8
Multiple CH, Multiple SF	100%	100%	100%	100%	100%	100%	99%
Multiple CH, Fixed-SF	100%	100%	100%	100%	100%	100%	100%
Single CH, Multiple SF	100%	100%	100%	100%	100%	–	–
Single CH, Fixed-SF	48%	32%	24%	19%	16%	13%	12%

With separation of either SF or CH between packets, LoRa gateway is able to demodulate collided packets efficiently.

node, CH1 has three nodes set on three orthogonal SFs. A transmission of this sort is seen by the concentrator as a concurrent transmission of six packets via four channels.

In addition, Figure 24 also leads to validate the theoretical relationship between T_{sym} and SF as predicted by Equation (1). According to Equation (1), the symbol durations for $SF7$, $SF9$, and $SF11$ should be ~1, ~4, and ~16ms, respectively, which corresponds to doubling of T_{sym} per each incrementing SF. Therefore, T_{sym} for $SF11$ should be 16 times T_{sym} of $SF7$. The visualized symbols on CH4 clearly attest to this statement. For example, during a single $SF11$ chirp, there exists 16 $SF7$ and 4 $SF9$ chirps. However, this should not lead to the conclusion that for a given payload, LoRa modulation doubles the dwell time for incrementing SFs. This is due to zero padding causing different number of data bits per each SF defined in the LoRa modulation resulting in a different number of total symbols for the same payload.

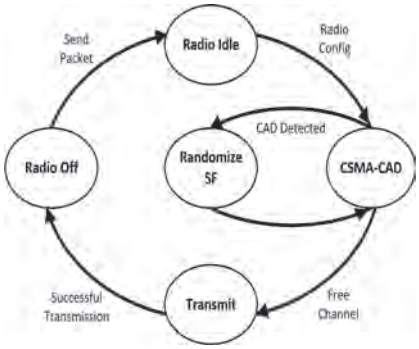
Having highlighted the advantages of orthogonal channels in LoRa, it can be observed that successful concurrent transmissions need not be limited to physically separated channels. Next, we estimate the extent of this concurrency of a standard IC880A LoRa concentrator.

To do this, we perform four experiments. In the first, we tie eight nodes to eight distinct channels. We program each node to continuously transmit 100 packets on a randomly selected SF. In all, to ensure continuous concurrency throughout the experiment, each transmission was time synchronized across all nodes. This synchronization was required to provide sufficient time to a node that opted to transmit at a higher SF (consuming a higher airtime) to finish the transmission. Since this experiment ensured eight packets in air at any given time, it can be used to validate Semtech's claim that the SX1301 LoRa concentrator can decode and demodulate eight packets at any given time. In the second, the same experiment was repeated by fixing all transmissions SF to SF7 on eight different channels. Results from both experiments depicted in the first two rows of Table 6 attest to the aforementioned claim by Semtech.

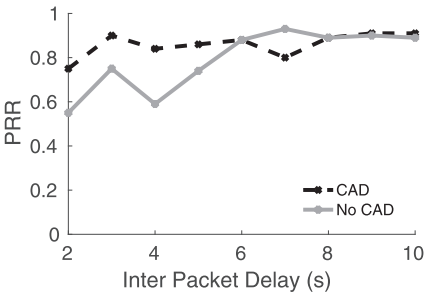
In the third, we test the concentrators capacity to receive orthogonal transmissions. We tie six nodes to six distinct SFs and program them to continuously transmit 100 packets on the same channel. The limitation on the number of nodes was due to the limitation on available SFs. Again, time synchronization between nodes ensured continuous concurrency throughout the experiment. As expected, the results indicated 100% PRR. Similarly, in the fourth, we transmit non-orthogonal packets within same channel. Our results confirm the disruptiveness of non-orthogonal transmissions. The results of third and fourth experiments are depicted in third and fourth rows in Table 6.

A Potential CSMA Mechanism for LoRa

An ideal mechanism to avoid potential collisions in LoRa is to sense the channel for non-orthogonal SFs prior to transmission. If a LoRa transceiver is able to detect such transmissions, then it forms the foundation to formulate an ideal CSMA mechanism for LoRa. Unfortunately, the SX1276 series LoRa transceivers limit such sensing to the preamble and call it the Carrier Activity Detection (CAD)-Mode [45]. Despite the limited functionality of CAD-Mode, we leverage the CAD-Mode to



(a) The CSMA-CAD mechanism illustrated as a state diagram.



(b) Comparison of CSMA-CAD and No-CSMA mechanisms for varying T_{pkt}. PL=10B, preamble length=8 and #Node=50.

Fig. 25. CSMA-CAD states and experiment results.

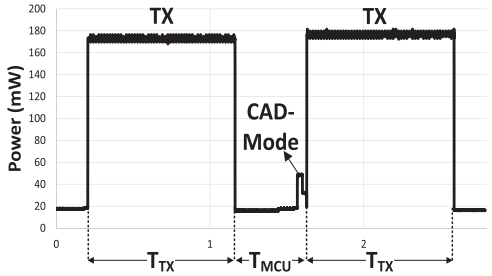
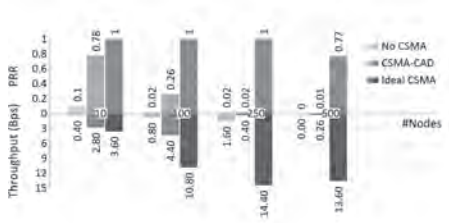


Fig. 26. No-CSMA vs. CSMA-CAD energy comparison.

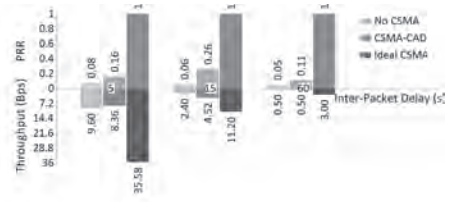
form CSMA-CAD and investigate the effectiveness of utilizing it as a potential collision avoidance mechanism. Although longer preambles could significantly increase the effectiveness of CSMA-CAD mechanism, without further changes on the concentrator, we confine our experiments to eight preamble symbols mandated in the LoRaWAN standard. CAD-Mode requires a duration of two symbols to complete. During the CAD process, the radio first performs a receive operation for a duration of a single symbol followed by a computation duration of another symbol. This CSMA-CAD process for an end node is described by Figure 25(a).

We then designed an experiment to test whether incorporating CAD-Mode is beneficial in a real-life environment. To do this, 50 nodes were fixed to a single channel and were programmed to transmit 100 packets of 10 Bytes payload. Each node transmitted 100 packets randomly within an inter-packet delay of T_{pkt}. A random start delay ensured the distribution of transmissions across T_{pkt}, which allowed the control of network density. We computed PRR for each experiment and repeated the same for T_{pkt} ranging from 2 to 10 seconds. A payload of 10 Bytes were chosen and the longest airtime corresponding to the airtime of SF12 was ensured to be less than T_{pkt}.

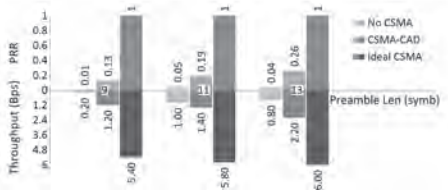
As indicated by the experiment results in Figure 25(b) the CAD-Mode enabled significant improvements to PRR under high network density conditions, i.e., when T_{pkt} is low. Further, we also determined the highest possible energy overhead (SF12 with longest T_{sym}) due to CAD-Mode to be at only 1.6963mJ. We present below a comparison of power profiles for both modes in Figure 26 transmitting a payload of 4 Bytes under SF12 at 5dBm. The peak indicated on the second transmission represents the power overhead of CSMA-CAD. That is, CSMA-CAD sensing and applying a different SF. As ideal CSMA protocol for LoRa should be able to sense the ongoing Spreading



(a) PRR vs #Nodes where preamble=8, payload=6B and Inter-packet Delay fixed at 15s.



(b) PRR vs Inter-packet Delay where preamble=8, payload=6B and number of Nodes fixed to 100.



(c) PRR vs Preamble Length where payload=6B, Inter-packet Delay=15s and number of Nodes fixed to 100.

Fig. 27. Simulation of a LoRa network under No-CSMA, CSMA-CAD, and Ideal-CSMA mechanisms. Although Ideal-CSMA mechanism shows promising results, hidden terminal problem and synchronous symbol detection would still cause packet collisions.

Factor at any point of payload, not just within the preamble. Nevertheless, based on our experimental results, it can be seen that performance improvements are still possible with the CSMA-CAD mechanism.

We then extend the boundaries of this experiment by means of a simulation in an effort to test the effect of varying number of nodes, T_{pkt}, and preamble length on the PRR. The simulation considers an erasure channel and compares the three CSMA mechanisms: (1) No-CSMA, (2) CSMA-CAD, and (3) Ideal-CSMA. Despite the obvious advantages that come through an Ideal-CSMA mechanism, CSMA-CAD still provides significant performance improvement under dense network conditions similar to experiment results.

It can be seen from the results that the Ideal-CSMA mode always achieves a full-packet reception ratio, except in Figure 27(a), where the number of nodes reached up to 500. This is understandable as many nodes perform symbol sensing, it is possible that a few performed synchronous symbol detection and transmitted simultaneously resulting in collisions. Despite the existence of this effect within a simulated environment, the same phenomena can take place within real-life environments causing potential decrements in PRR. Last, Figure 27(c) depicts that the Ideal-CSMA mechanism is not significantly affected by the number of preamble symbols. However, the impact is significant for a CSMA-CAD network, which achieves a doubled performance in PRR with only four additional preamble symbols. At the same time, as expected, the No-CSMA mechanism reflects an inverse performance affected by the increased preamble symbols.

Semtech has also began to answer the need for a better CSMA mechanism in LoRa chipsets by announcing a new chipset, which allows CSMA mechanism beyond CAD [57]. With improved CSMA mechanisms, researchers would be able to design better MAC protocols, which would reduce the number of possible collisions while enhancing network quality.

4.4 Revisiting LoRa PHY

Understanding LoRa PHY would open a path to enabling many applications such as passive localization [53], cooperative transmission [14, 15], co-existing and complementing MAC protocol [19], and so on. To understand LoRa PHY, one has to start from the encoding and modulation process of a packet.

For a given payload, LoRa PHY integrates several encoding mechanisms to improve the over-the-air resiliency prior to modulation. This encoding process involves Forward Error Correction (FEC), Interleaving, Whitening, and Gray Coding, in that order [48]. The process of modulation is responsible for integrating data bits into "base chirps" also known as "linear chirps," explained duly. We provide insights to this process under this section.

LoRa Modulation and Demodulation

The complex baseband representation of a single frequency (pure tone) can be expressed as follows, where f_0 refers to the frequency of tone and ϕ represents a possible phase shift:

$$f_{tone}(t) = e^{j(2\pi f_0 t + \phi)}. \tag{10}$$

In contrast, a linear chirp or an "unmodulated" chirp sweeps through a given channel bandwidth BW from f_{start} to f_{end} by continuously changing the frequency at rate m. Equation (11) expresses such a chirp where f_0 represents the starting frequency at $t = 0$; hence, $mt + f_0$ represents the instantaneous frequency at any given time t [32]:

$$f_{chirp}(t) = e^{j(2\pi(mt + f_0)t + \phi)}. \tag{11}$$

A *rf symbol* in LoRa is a single chirp that sweeps the bandwidth BW. It can be seen that to sweep the bandwidth BW in exactly T_{sym} duration, the rate of change of frequency m of the chirp should be $m = \frac{BW}{T_{sym}}$. The symbol duration T_{sym} is defined as $T_{sym} = \frac{2^{SF}}{BW}$ in Semtech's LoRa patent [50]. This implies that as long as the BW is fixed, a higher SF requires a longer T_{sym} duration. A LoRa packet consists of a combination of such unmodulated as well as modulated chirps. The unmodulated formulate the preamble and the Start Frame Delimiter (SFD), whereas the modulated form header, payload, and CRC.

To modulate data bits into a base chirp, its instantaneous frequency is changed exactly once. For any given SF, a modulated chirp will consist of a single shift out of a possible $2^{SF} - 1$. This implies that depending on the SF, a single modulated LoRa chirp carries SF number of bits of information. In other words, an integer in the range of 0 to $2^{SF} - 1$ is represented using $2^{SF} - 1$ possible frequency shifts. During the process of demodulation, each frequency shift in the data chirp is recognized as a separate FFT bin, which relates back to the original integer. In a more technical perspective, the process of modulation can be visualised in the time domain as follows.

After performing FEC, Interleaving, and Whitening on the payload, to modulate the resulting encoded data into *data chirps*, the data is divided into SF-sized bit chunks. Each chunk, of SF bits, represents an integer i within the range 0 to $2^{SF} - 1$. i is then modulated to a base chirp by introducing a time shift of $\hat{t} = Gray^{-1}(i)\frac{T}{2_{SF}}$ [48] to the signal presented in equation Equation (11), where $Gray^{-1}$ stands for the reverse of Gray operation in Reference [18].

Later, at the receiver, each received chirp is multiplied by a locally generated conjugate *base chirp* of same rate of change of frequency m, known as de-chirping. Multiplying two in-phase base chirps of same m but of opposite signs results in an argmax at the bin corresponding to 0Hz in a FFT that is of 2^{SF} bins wide, due to destructive superposition of these two waveforms [33]. However,

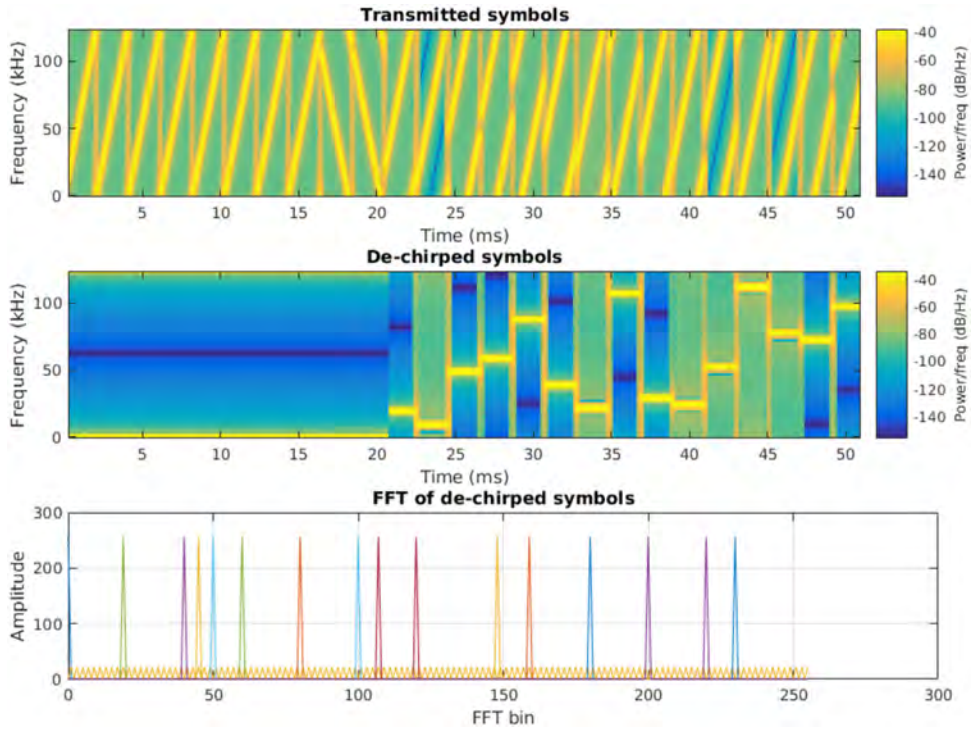


Fig. 28. LoRa demodulation to FFT bins.

when a received *data chirp* undergoes de-chirping, the argmax of the FFT for each received chirp will occur at one of 2^{SF} bins. This bin can be directly correlated to the originally modulated integer i, which is in the range of 0 to $2^{SF} - 1$.

However, it should be mentioned that for a given difference in phase ϕ between the received and the locally generated chirp, FFT bins upon de-chirping operation may contain an offset. This problem can be rectified by consulting the information from preamble and SFD bits mandated to the front of every LoRa payload.

To further illustrate the process of demodulation, Figure 28(a) closely represents a received SF7 LoRa signal of 15 payload symbols. Figure 28(b) presents the same signal upon de-chirping, while Figure 28(c) presents the FFT bins that correspond to i. Since the signal is SF8 modulated, each data chirp can only take a value between 0 and 127 and the FFT bins are also limited to the same range. Therefore, the FFT width is set to 2^8 and each bin in Figure 28(c) represents the data previously modulated into each data chirp after the preamble and SFD in Figure 28(a).

Doppler Effect

When a transmitter or a receiver move relative to each other, the apparent frequency shift on the received signal is known as the Doppler's effect. Depending on the extent of this effect, the signal is either received or discarded. CSS, however, is widely known to be immune to Doppler effect [56, 65]. LoRa, being a close variant of CSS, inherits a degree of resilience from it. Under this section, we conduct a series of experiments to study possible effects caused due to Doppler shift on LoRa's modulation under practical circumstances.

Table 7. Experiment Results for Doppler Test with Varying Speeds

Speed(kmph)	Number of RX/TX Packets		
	Approaching	Intermediate	Leaving
50	1/1	1/1	1/2
60	3/4	1/1	3/3
70	3/3	1/1	3/3
80	2/2	1/1	1/2

This apparent change in frequency of a LoRa chirp due to Doppeler's shift can be integrated to LoRa's modulation equation as follows:

$$f_{chirp}(t) = e^{j(2\pi(mt^2+f_0t+\Delta f_d t)+\phi)}, \tag{12}$$

where Δf_d is the change frequency caused due to Doppler effect. Under general use cases, where end nodes move at a velocity v_{en} relative to a stationary LoRa gateway, this Δf_d approximates to $\Delta f_d = \frac{v_{en}}{C} f_{chirp}$, where f_{chirp} represents the instantaneous chirp frequency. In the case of CSS, this Δf_d causes the autocorrelation peak on the receiver side to shift in time and this time shift is approximated by $\frac{\Delta f_d}{m}$ [65]. The same approach can be used to determine the most susceptible SFs in LoRa modulation under Doppler effect. It can be seen for smaller chirp rates m, the time shift is higher. This concludes that SF12 is most effected while SF7 is the least.

To quantify the effect of Doppler shift on LoRa chirps, we set-up a mobile LoRa gateway and an SDR setup by the roadside and attach a node to a car used as moving transmitter. We drive the car at varying speeds ranging from 50, 60, 70, and 80kmph on a highway. Extreme care was taken at all times to maintain persistent speed of the car and line of sight to the gateway during transmissions. Each transmission with 50 bytes were performed on SF12 with a packet duration of 2.35s to ensure sufficient time for recording a packet with both approaching and passing states. Each round maintains a fixed speed with the vehicle approaching the gateway, in-between, and last, passing the gateway. More specifically, each transmission consisted a sequence number. A gateway was placed by the highway ensuring LOS with the car while a second received records the transmissions from inside the vehicle without Doppler's effects.

Our results indicate strong packet reception (>85%) at gateway placed by the highway for all tested speeds and Table 7 summarize the results of the experiment for all speeds.

Further, we also compare recorded transmissions from within the car with the transmissions recorded using the receiver placed by the highway using the SDR setup seeking for observable Doppler effects. We present a comparison of two snapshots of LoRa chirps transmitted at 80kmph in Figure 29. Visually, both recordings offered no observable difference and similar results were observed for other speeds. Contrary to the findings in Reference [39], which reported a significant influence on PRR even at speed 8kmph, our results show no observable influence on PRR nor spectogram records, even at the high speed of 80kmph.

Although LoRa technology is robust to a high degree against Doppler effect, it may still be possible to capture frequency deviations in the chirps due to Doppler effects and predict the speed of moving end nodes [22, 38].

5 RELATED WORKS AND CONCLUSION

In this article, we have conducted experiments to verify common claims made on LoRa and derived models in accordance with said promises.

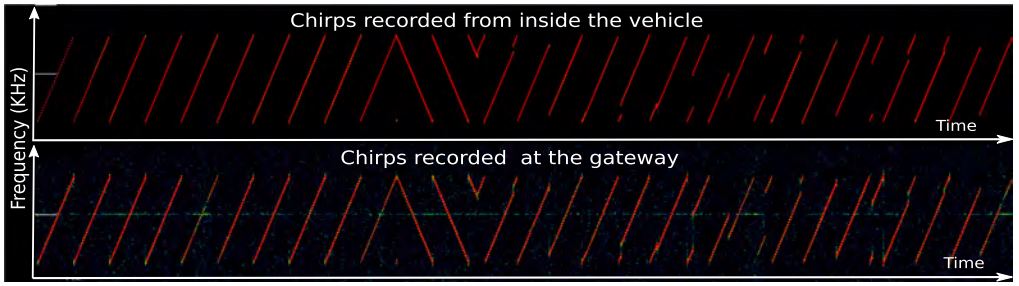


Fig. 29. A LoRa transmission recorded from inside the vehicle (top) and at the gateway (bottom) for a payload of 50 Bytes at SF12. The vehicle was driving pass the gateway at the speed of 80kmph. No significant difference on the chirps can be observed from comparing the two spectrogram.

A significant amount of work has been focused on differences between LoRa and similar technologies [12, 25, 28, 36, 55, 63], including batteryless operation of LoRa-enabled devices [40, 60]. Few others have also focused on surveying various aspects of the LoRa network stacks [26, 44]. Our work differs from those as it concludes a series of experiments that help derive answers to questions regarding LoRa's promises and also beyond.

In verifying LoRa's communication distance, this article answers important questions, such as: "How far can a LoRa end node transmit?"; "What parameters should a node use for optimal coverage?"; and so on. Through multiple experiments under a variety of environments, the results presented in this article show that LoRa transmissions are capable of transmitting beyond 10km under LoS environments. However, with the presence of obstacles blocking LoS, LoRa's coverage declines drastically. Moreover, in metropolitan city environments among high-rise buildings, LoRa's coverage drops to 3km. This article also quantifies the importance of SF over other parameters and provides both researchers and system adopters a rule of thumb to always select the lowest SF whenever possible. The results in this article agree with the those presented in References [4, 29, 30, 37, 62] for coverage in open environments and References [20, 42] for coverage in indoor environments. In contrast to Reference [13] where signal propagation is modeled for different environments, this article tries to model the effect of different parameters on coverage under varying environments.

Another important question this article tries to answer is "How do modulation parameters affect lifetime of nodes?" In doing so, this article proposes a model to quantify the lifetime of a node by predicting the energy consumption during a transmission. The proposed model was derived from real measurement data across multiple chipsets. With it, the article concludes that a node could only sustain its operation to the order of years with careful parameter selection, extremely low duty cycle setting, and meticulous selection of MCUs. Moreover, LoRaWAN imposes on average 198% of overhead to the energy budget of a node by increasing both payload size and node active duration. A similar study was done in Reference [9], which proposed a model to compute the energy expended by a node during a transmission cycle; however, our work found that the expended energy is non-linear and can be modeled. Moreover, Petajajarvi et al. [43] highlight the power consumption of a node as a whole. Our work takes this step further by dissecting a transmission cycle along with its sub-components responsible for the lifetime of a node.

A fundamental question raised prior to deploying a LoRa network would be "How many nodes can a gateway support?" This article performed multiple experiments to quantify the node capacity of a gateway through (1) quantifying the number of supported nodes for a single SF network on a single channel, (2) quantifying the number of supported nodes for a single channel with

multiple SFs, and (3) exploring the overheads and gains of LoRaWAN. Counterintuitively, a channel with only SF7 supports a lower number of nodes as compared to a channel with only SF12 due to high number of packet collisions caused by high number of inter-packet interference from the low duty cycle of SF7. However, a mixed SFs network performs better if more SF7 packets are present in the network. This is due to the concurrent demodulation capability of the gateway, which demodulates collided packets in the orthogonal space. While a single SF channel would be full of non-orthogonal packet collisions, a mixed SF channel would innately leverage orthogonality of SFs to avoid collisions along with capture effect [21] to increase both throughput and the number of supported nodes. Results of the experiments indicate that a single-channel gateway with multiple SFs could support >14,000 nodes. While simply extending the capability of a single channel to multiple channels would not be logical, however, a single channel with six SFs only exploits six out of eight concurrent demodulators designed in the concentrator chipset. Additionally, as the standard MAC protocol for LoRa , LoRaWAN overhead does not provide equivalent returns. On top of the high-energy overhead due to encryption and RX delays, significantly large LoRaWAN overhead due to header information diminishes the throughput gain it brings. Albeit similar to References [2, 5, 6, 8], which focus on the network capacity of LoRaWAN, this article mainly explores the number of nodes supported by LoRa itself and hopes to serve as a baseline for future studies.

Looking further into the combined experiment results, this article answers the question every system adopter would like to know: "What is the optimal setting for a node?" To answer this question, the article proposes a simple search algorithm to find the optimal setting and also provides a rule that suggests that TX Pow is a more efficient parameter in terms of end node lifetime while SF is a more efficient parameter in terms of coverage. While there exists multiple SF and TX Pow settings to reach a desired distance, settings with lower SF and higher TX Pow should always be preferred, which reduces the search space by 79%. With this significant reduction in the search space, system adopters would be able to survey deployment areas more efficiently while researchers would be able to design more efficient rate adaptation algorithms. Reynders et al. [47] propose a parameter selection algorithm by evaluating individual path loss values of each node on each channel assessed by the gateway, which then assign the selected parameter to the end node through downlink transmissions. Results in this article could compliment Reynders et al.'s algorithm by limiting the search space.

Although a LoRa concentrator's capability to demodulate orthogonally colliding packets is in contrast to other LPWAN technologies, a LoRa gateway could still experience collisions from packets within non-orthogonal data rates. Studies like CHOIR [15] has proposed a method to separate such collisions by leveraging imperfections present within an end node's hardware. However, collisions could be averted by leveraging a CSMA mechanism prior to transmission. CAD mode in the SX127X chipset is capable on sensing a potentially colliding packet during the preamble. This article exploits this mode by implementing a simple CSMA mechanism and discovers that paying a small price in energy budget (<1.70mJ) for CSMA-CAD provides up to 20% PRR improvement. A simulation was also conducted to investigate the possible gain of an ideal CSMA mechanism. The simulation predicts that an ideal CSMA mechanism can increase the throughput up to 56× compared to CSMA-CAD.

In summary, this article has answered common questions system adopters and researchers have about LoRa and verifies the promises Semtech has made in terms of transmission distance, end node lifetime, and node capacity. It further provides a deeper understanding on the effect of modulation parameters on the aforementioned promises, which could aid system designers in designing a better MAC protocols for LoRa. Last, a simple experiment to test the resiliency of LoRa against the Doppler effect also provided encouraging results about LoRa modulation.

REFERENCES

[1] LTE Release 13. 2018. Release 13. Retrieved from http://www.3gpp.org/release-13.

[2] Ferran Adelantado, Xavier Vilajosana, Pere Tuset-Peiro, Borja Martinez, Joan Melia-Segui, and Thomas Watteyne. 2017. Understanding the limits of LoRaWAN. *IEEE Commun. Mag.* 55, 9 (2017), 34–40.

[3] Wi-Fi Alliance. 2018. Wi-Fi HaLow | Wi-Fi Alliance. Retrieved from https://www.wi-fi.org/discover-wi-fi/wi-fi-halow.

[4] Aloÿs Augustin, Jiazi Yi, Thomas Clausen, and William Mark Townsley. 2016. A study of LoRa: Long-range and low-power networks for the internet of things. *Sensors* 16, 9 (2016), 1466.

[5] Eyuel D. Ayele, Chiel Hakkenberg, Jan Pieter Meijers, Kyle Zhang, Nirvana Meratnia, and Paul J. M. Havinga. 2017. Performance analysis of LoRa radio for an indoor IOT applications. In *Proceedings of the IEEE International Conference on Internet of Things for the Global Community (IoTGC'17)*.

[6] Dmitry Bankov, Evgeny Khorov, and Andrey Lyakhov. 2016. On the limits of LoRaWAN channel access. In *Proceedings of the International Conference on Engineering and Telecommunication (EnT'16)*. 29–30.

[7] Steve Battle and Benedict Gaster. 2017. LoRaWAN Bristol. In *Proceedings of the 21st International Database Engineering and Applications Symposium*. ACM, 287–290.

[8] Norbert Blenn and Fernando Kuipers. 2017. LoRaWAN in the wild: Measurements from the things network. *arXiv preprint arXiv:1706.03086*.

[9] Taoufik Bouguera, Jean-François Diouris, Jean-Jacques Chaillout, Randa Jaouadi, and Guillaume Andrieux. 2018. Energy consumption model for sensor nodes based on LoRa and LoRaWAN. *Sensors* 18, 7 (2018).

[10] Michael Coracin and Matthieu Leurent. 2017. GitHub—Lora-net/lora_gateway: Driver/HAL to build a gateway using a concentrator board based on Semtech SX1301 multi-channel modem and SX1257/SX1255 RF transceivers. Retrieved from https://github.com/Lora-net/lora_gateway.

[11] CRC Computation. 2013. Implementing Data Whitening and CRC Calculation in Software on SX12XX Devices. Rev. 1. https://www.semtech.com/uploads/documents/AN1200.18_STD.pdf.

[12] Jonathan de Carvalho Silva, Joel J. P. C. Rodrigues, Antonio M. Alberti, Petar Solic, and Andre L. L. Aquino. 2017. LoRaWAN-A low-power WAN protocol for internet of things: A review and opportunities. In *Proceedings of the 2nd International Multidisciplinary Conference on Computer and Energy Science (SpliTech'17)*. IEEE, 1–6.

[13] Dalibor Dobrilović, Milan Malić, Dušan Malić, and Srđan Sladojević. 2017. Analyses and optimization of Lee propagation model for LoRa 868 MHz network deployments in urban areas. *J. Eng. Manage. Compet.* 7, 1 (2017), 55–62.

[14] Wan Du, Jansen Christian Liando, Huanle Zhang, and Mo Li. 2017. Pando: Fountain-enabled fast data dissemination with constructive interference. *IEEE/ACM Trans. Netw.* 25, 2 (2017), 820–833.

[15] Rashad Eletreby, Diana Zhang, Swarun Kumar, and Osman Yağan. 2017. Empowering low-power wide-area networks in urban settings. In *Proceedings of the Conference of the ACM Special Interest Group on Data Communication*. ACM, 309–321.

[16] Eric Gourlaouen, Johan Stokking, and Hylke Visser. 2017. GitHub—TheThingsNetwork/packet_forwarder: Packet forwarder for Linux-based gateways. Retrieved from https://github.com/TheThingsNetwork/packet_forwarder.

[17] Claire Goursaud and Jean-Marie Gorce. 2015. Dedicated networks for IoT: PHY/MAC state of the art and challenges. *EAI Endorsed Transactions on Internet of Things*. DOI: https://doi.org/10.4108/eai.26-10-2015.150597.

[18] Frank Gray. 1946. Pulse code communication. U.S. Patent US2632058A.

[19] C. Gu, R. Tan, X. Lou, and D. Niyato. 2018. One-hop out-of-band control planes for low-power multi-hop wireless networks. In *Proceedings of the IEEE Conference on Computer Communications (INFOCOM'18)*. 1187–1195. DOI: https://doi.org/10.1109/INFOCOM.2018.8486301

[20] Jetmir Haxhibeqiri, Abdulkadir Karaagac, Floris Van den Abeele, Wout Joseph, Ingrid Moerman, and Jeroen Hoebeke. 2017. LoRa indoor coverage and performance in an industrial environment: Case study. In *Proceedings of the 22nd IEEE International Conference on Emerging Technologies and Factory Automation (ETFA'17)*. IEEE, 1–8.

[21] Jetmir Haxhibeqiri, Floris Van den Abeele, Ingrid Moerman, and Jeroen Hoebeke. 2017. Lora scalability: A simulation model based on interference measurements. *Sensors* 17, 6 (2017), 1193.

[22] C. Huang, T. Teng, and D. Sun. 2016. Low-speed moving target detection of single frame image based on Doppler shift estimation. In *Proceedings of the IEEE/OES China Ocean Acoustics (COA'16)*. 1–4. DOI: https://doi.org/10.1109/COA.2016.7535703

[23] IC880a. 2015. WiMOD iC880A. Ver. 0.5. https://shop.imst.de/media/pdf/22/67/a8/iC880A_Datasheet_V0_50.pdf.

[24] Inair9b. [n.d.]. inAir9 Datasheet and Schematics. http://modtronix.com/prod/imod/inair9/inair9_r1.pdf.

[25] Gabor Kecskemeti, Giuliano Casale, Devki Nandan Jha, Justin Lyon, and Rajiv Ranjan. 2017. Modelling and simulation challenges in internet of things. *IEEE Cloud Comput.* 4, 1 (2017), 62–69.

[26] Oratile Khutsoane, Bassey Isong, and Adnan M. Abu-Mahfouz. 2017. IoT devices and applications based on LoRa/LoRaWAN. In *Proceedings of the 43rd Annual Conference of the IEEE Industrial Electronics Society (IECON'17)*. IEEE, 6107–6112.

[27] Alexandru Lavric and Adrian Ioan Petrariu. 2018. LoRaWAN communication protocol: The new era of IoT. In *Proceedings of the International Conference on Development and Application Systems (DAS'18)*. IEEE.

[28] Alexandru Lavric and Valentin Popa. 2017. A LoRaWAN: Long-range wide-area networks study. In *Proceedings of the International Conference on Electromechanical and Power Systems (SIELMEN'17)*. IEEE, 417–420.

[29] Lingling Li, Jiuchun Ren, and Qian Zhu. 2017. On the application of LoRa LPWAN technology in sailing monitoring system. In *Proceedings of the 13th Annual Conference on Wireless On-demand Network Systems and Services (WONS'17)*. IEEE, 77–80.

[30] Alexander Liljegren and Robin Franksson. 2018. Measuring a LoRa Network: Performance, Possibilities and Limitations. In *Proceedings of the 18th International Conference, NEW2AN 2018, and 11th Conference (ruSMART'18), St. Petersburg, Russia*. 116–128. DOI: 10.1007/978-3-030-01168-0_11

[31] LoRaWAN. 2017. LoRaWAN 1.1 Specification. Ver. 1.1. https://lora-alliance.org/sites/default/files/2018-04/lorawantm_specification_-v1.1.pdf.

[32] Steve Mann and Simon Haykin. 1991. The chirplet transform: A generalization of Gabor's logon transform. In *Vision Interface*, Vol. 91. 205–212.

[33] Knight Mathew and Seeber Balint. 2016. Decoding LoRa: Realizing a modern LPWAN with SDR. In *Proceedings of the GNU Radio Conference*. GNU Radio.

[34] Modulation. 2015. LoRa Modulation Basics. Rev. 2. https://www.semtech.com/uploads/documents/an1200.22.pdf.

[35] Pierre Neumann, Julien Montavont, and Thomas Noël. 2016. Indoor deployment of low-power wide-area networks (LPWAN): A LoRaWAN case study. In *Proceedings of the IEEE 12th International Conference on Wireless and Mobile Computing, Networking and Communications (WiMob'16)*. IEEE, 1–8.

[36] Umber Noreen, Ahcène Bounceur, and Laurent Clavier. 2017. A study of LoRa low-power and wide-area network technology. In *Proceedings of the International Conference on Advanced Technologies for Signal and Image Processing (ATSIP'17)*. IEEE, 1–6.

[37] Rúben Oliveira, Lucas Guardalben, and Susana Sargento. 2017. Long range communications in urban and rural environments. In *Proceedings of the IEEE Symposium on Computers and Communications (ISCC'17)*. IEEE, 810–817.

[38] I. Omelchuk, I. Prokopenko, and I. Chyrka. 2016. Multichannel target speed estimation by a colocated Doppler-pulse MIMO radar. In *Proceedings of the International Conference Radio Electronics Info Communications (UkrMiCo'16)*. 1–5. DOI: https://doi.org/10.1109/UkrMiCo.2016.7739601

[39] Dhaval Patel and Myounggyu Won. 2017. Experimental study on low-power wide-area networks (LPWAN) for mobile internet of things. In *Proceedings of the IEEE 85th Vehicular Technology Conference (VTC'17)*. IEEE, 1–5.

[40] Yao Peng, Longfei Shangguan, Yue Hu, Yujie Qian, Xianshang Lin, Xiaojiang Chen, Dingyi Fang, and Kyle Jamieson. 2018. PLoRa: A passive long-range data network from ambient LoRa transmissions. In *Proceedings of the Conference of the ACM Special Interest Group on Data Communication*. ACM, 147–160.

[41] Juha Petäjäjärvi, Konstantin Mikhaylov, Marko Pettissalo, Janne Janhunen, and Jari Iinatti. 2017. Performance of a low-power wide-area network based on LoRa technology: Doppler robustness, scalability, and coverage. *Int. J. Distrib. Sensor Netw.* 13, 3 (2017), 1550147717699412.

[42] Juha Petäjäjärvi, Konstantin Mikhaylov, Antti Roivainen, Tuomo Hanninen, and Marko Pettissalo. 2015. On the coverage of LPWANs: Range evaluation and channel attenuation model for LoRa technology. In *Proceedings of the 14th International Conference on ITS Telecommunications (ITST'15)*. IEEE, 55–59.

[43] Juha Petäjäjärvi, Konstantin Mikhaylov, Rumana Yasmin, Matti Hämäläinen, and Jari Iinatti. 2017. Evaluation of LoRa LPWAN technology for indoor remote health and wellbeing monitoring. *Int. J. Wireless Info. Netw.* 24, 2 (2017), 153–165.

[44] Tara Petrić, Mathieu Goessens, Loutfi Nuaymi, Laurent Toutain, and Alexander Pelov. 2016. Measurements, performance and analysis of LoRa FABIAN, a real-world implementation of LPWAN. In *Proceedings of the IEEE 27th Annual International Symposium on Personal, Indoor, and Mobile Radio Communications (PIMRC'16)*. IEEE, 1–7.

[45] Congduc Pham. 2018. Investigating and experimenting CSMA channel access mechanisms for LoRa IoT networks. In *Proceedings of the IEEE Wireless Communications and Networking Conference (WCNC'18)*. IEEE, 1–6.

[46] Power monitor. 2014. Mobile Device Power Monitor Manual. Rev. 1.14. http://msoon.github.io/powermonitor/PowerTool/doc/LVPM%20Manual.pdf.

[47] Brecht Reynders, Wannes Meert, and Sofie Pollin. 2017. Power and spreading factor control in low-power wide-area networks. In *Proceedings of the IEEE International Conference on Communications (ICC'17)*. IEEE, 1–6.

[48] Pieter Robyns, Peter Quax, Wim Lamotte, and William Thenaers. 2018. A Multi-channel software decoder for the LoRa modulation scheme. In *Proceedings of the 3rd International Conference on Internet of Things, Big Data and Security—Volume 1 (IoTBDS'18)*. INSTICC, SciTePress, 41–51.

[49] Tom Rondeau, Josh Blum, Johnathan Corgan, Eric Blossom, and Sebastian Koslowski. [n.d.]. GitHub-gnuradio/gnuradio: GNU Radio. Retrieved from https://github.com/gnuradio/gnuradio.

[50] Olivier Bernard André Seller. 2017. Wireless communication method. U.S. Patent 9,647,718.

[51] Olivier Bernard André Seller and Nicolas Sornin. 2016. Low power long range transmitter. U.S. Patent 9,252,834.
[52] Semtech. 2012. Semtech Acquires Wireless Long Range IP Provider Cycleo | Semtech Corporation. Retrieved from http://investors.semtech.com/releasedetail.cfm?ReleaseID=655335.
[53] Longfei Shangguan, Zheng Yang, Alex X. Liu, Zimu Zhou, and Yunhao Liu. 2017. STPP: Spatial-temporal phase profiling-based method for relative RFID tag localization. *IEEE/ACM Trans. Netw.* 25, 1 (2017), 596–609.
[54] Sigfox. 2018. Sigfox—The Global Communications Service Provider for the Internet of Things (IoT). Retrieved from https://www.sigfox.com/.
[55] Rashmi Sharan Sinha, Yiqiao Wei, and Seung-Hoon Hwang. 2017. A survey on LPWA technology: LoRa and NB-IoT. *ICT Express* 3, 1 (2017), 14–21.
[56] Andreas Springer, Mario Huemer, Leonhard Reindl, Clemens C. W. Ruppel, Alfred Pohl, Franz Seifert, Wolfgang Gugler, and Robert Weigel. 1998. A robust ultra-broad-band wireless communication system using SAW chirped delay lines. *IEEE Trans. Microwave Theory Tech.* 46, 12 (1998), 2213–2219.
[57] SX1261. 2017. SX1261/2 Long Range, Low Power, sub-GHz RF Transceiver. Rev. 1.1. https://www.semtech.com/uploads/documents/DS_SX1261-2_V1.1.pdf.
[58] SX1276. 2016. SX1276/77/78/79—137 MHz to 1020 MHz Low Power Long Range Transceiver. Rev. 5. https://www.semtech.com/uploads/documents/DS_SX1276-7-8-9_W_APP_V5.pdf.
[59] SX1301. 2017. SX1301 Datasheet. Ver. 2.3. https://www.semtech.com/uploads/documents/sx1301.pdf.
[60] Vamsi Talla, Mehrdad Hessar, Bryce Kellogg, Ali Najafi, Joshua R. Smith, and Shyamnath Gollakota. 2017. LoRa backscatter: Enabling the vision of ubiquitous connectivity. *Proc. ACM Interact. Mobile Wear. Ubiq. Tech.* 1, 3 (2017), 105.
[61] USRP N210. [n.d.]. USRP N200/N210 Networked Series. https://www.ettus.com/content/files/Ettus_N200-210_DS_Flyer_HR_2.pdf.
[62] Nuttakit Vatcharatiansakul, Panwit Tuwanut, and Chotipat Pornavalai. 2017. Experimental performance evaluation of LoRaWAN: A case study in Bangkok. In *Proceedings of the 14th International Joint Conference on Computer Science and Software Engineering (JCSSE'17)*. IEEE, 1–4.
[63] Benny Vejlgaard, Mads Lauridsen, Huan Nguyen, István Z. Kovács, Preben Mogensen, and Mads Sorensen. 2017. Coverage and capacity analysis of sigfox, LoRa, gprs, and nb-iot. In *Proceedings of the IEEE 85th Vehicular Technology Conference (VTC'17)*. 4–7.
[64] Weightless. 2018. Weightless—Setting the Standard for IoT. Retrieved from http://www.weightless.org/.
[65] Peng Zhang and Hao Liu. 2006. An ultra-wide band system with chirp spread spectrum transmission technique. In *Proceedings of the 6th International Conference on ITS Telecommunications Proceedings*. IEEE, 294–297.

Received August 2018; revised October 2018; accepted November 2018